



Petrological and geochemical study of Birimian ultramafic rocks within the West African Craton: Insights from Mako (Senegal) and Loraboué (Burkina Faso) lherzolite/harzburgite/wehrlite associations

Ibrahima Labou, Mathieu Benoit, Lenka Baratoux, Michel Grégoire, Papa Moussa Ndiaye, Nicolas Thebaud, Didier Béziat, Pierre Debat

► To cite this version:

Ibrahima Labou, Mathieu Benoit, Lenka Baratoux, Michel Grégoire, Papa Moussa Ndiaye, et al.. Petrological and geochemical study of Birimian ultramafic rocks within the West African Craton: Insights from Mako (Senegal) and Loraboué (Burkina Faso) lherzolite/harzburgite/wehrlite associations. *Journal of African Earth Sciences*, 2020, 162, pp.103677. 10.1016/j.jafrearsci.2019.103677 . hal-02360226

HAL Id: hal-02360226

<https://hal.science/hal-02360226>

Submitted on 25 Nov 2020

HAL is a multi-disciplinary open access archive for the deposit and dissemination of scientific research documents, whether they are published or not. The documents may come from teaching and research institutions in France or abroad, or from public or private research centers.

L'archive ouverte pluridisciplinaire **HAL**, est destinée au dépôt et à la diffusion de documents scientifiques de niveau recherche, publiés ou non, émanant des établissements d'enseignement et de recherche français ou étrangers, des laboratoires publics ou privés.

1 **Petrological and geochemical study of Birimian ultrabasic rocks within the West African**
2 **Craton: insights from Mako (Senegal) and Loraboué (Burkina Faso)**
3 **Iherzolite/harzburgite/wehrlite associations.**

4

5 Ibrahima Labou^{a,b,c,*}, Mathieu Benoit^b, Lenka Baratoux^b, Michel Grégoire^b, Papa Moussa
6 Ndiaye^a, Nicolas Thebaud^d, Didier Béziat^b, Pierre Debat^b

7 ^a Department of Geology, Faculty of Science and Technology, Cheikh Anta Diop University, Dakar, Senegal

8 ^b Laboratory GET, University of Toulouse 3 Paul Sabatier, CNRS, IRD, UPS, (Toulouse), France

9 ^c Fundamental Institute of Black Africa (IFAN), Cheikh Anta Diop, Dakar, Senegal

10 ^d Centre for Exploration Targeting School of Earth and Environment, University of Western Australia

11

12 **Abstract**

13 In Archean and Paleoproterozoic greenstone belts, ultrabasic (UB) rock occurrences are
14 commonly found in close association within basic and differentiated magmatic series. In the
15 Kedougou inlier (West African Craton), UB rocks are interbeded within the Birimian (2.1 Ga)
16 Mako tholeiitic series (basalts, gabbros). UBs are typically lherzolite, harzburgite and wehrelite,
17 characterized by their cumulative textures and relative proportions of chromite, olivine,
18 clinopyroxene, amphibole ± orthopyroxene. Geochemical study (Major, REE and trace
19 elements in whole rocks and mineral (mainly clinopyroxene and amphibole) and Sr/Nd isotopic
20 records suggest the existence of different types of complexes. The first one consists of lherzolite
21 + harzburgite assemblages whereas the second one consists of isolated wehrelite massifs. Both
22 complexes highlight two different geodynamic environments, the first association being
23 significantly more juvenile or mantle-related than isolated wehrellites which show more evolved
24 geochemical signatures.

25 UB rocks (dunite + wehrelite) of Loraboué (greenstone belt of Boromo, Burkina Faso)
26 associated with calc-alkaline series display the same mineralogical composition as the Mako
27 UB rocks but exhibit a different whole rock composition characteristics of mature island-arc
28 magmas and showing U-shaped REE pattern for both clinopyroxene and host rock, and a clear
29 negative Nb anomaly.

30 The Mako UBs suggest that this portion of the Birimian crust was built in an oceanic context
31 evolving from a MORB-like domain to an increasingly mature volcanic arc domain.

32 **Keywords:** Ultrabasic rocks, West African Craton, Birimian, Geochemistry, Sr-Nd isotopes,
33 Paleotectonic setting

34

35 **1. Introduction**

36 In Archaean and Paleoproterozoic terranes, the petrogenetic models associated with genesis
37 of igneous rocks are essentially based on available data on basic (volcanic and plutonic), and
38 on granite-related lithologies, thanks to the extensive use of zircon isotopic signatures (U/Pb,
39 Lu/Hf). Their little occurrences and the scarcity of reliable UB geochemical analysis made them
40 rarely integrated into the geodynamic models (e.g., [Condie, 1994](#)). UB constitute only a minor
41 component of the Archean and Paleoproterozoic greenstone belts ([Furnes et al., 2015](#)).
42 Outcrops are rare, scattered, relatively small and petrographically and geochemically
43 disconnected from the main mafic and aciditic sequences. As a result, crustal evolution models
44 rarely integrate the geochemical characteristics of UB rocks to further constrain the evolution
45 of the Earth crust (e.g., [Albarede, 1998](#); [Condie, 2000](#); [Hawkesworth et al. 2013](#)).

46 There are several interpretations for the emplacement and preservation of ancient UB rock
47 suites and there is an extensive debate regarding the geodynamic processes of their formation
48 (compilation in [Olieroor et al., 2018](#)). The UB rocks have been interpreted as: (i) part of
49 ophiolitic complexes ([Furnes et al., 2015](#)); (ii) relics of Large Igneous Province-type Layered
50 Complex associated to deep continental crust ([Yu et al., 2015](#); [Grant et al., 2016](#)) or arcs settings
51 ([Jagoutz et al., 2006](#); [Burg et al., 2009](#)); (iii) roots of ultrabasic-basic (UB-B) arc complexes
52 like Alaskan-type ([Grant et al., 2016](#); [Yuan et al., 2017](#)). Moreover, their formation have been
53 associated with various geodynamic environments: i) back-arc suprasubduction zone ophiolite
54 ([Myers et al., 1996](#); [Furnes et al., 2015](#)); ii) plume-enhanced back-arc basin ([Pirajno and](#)
55 [Ocipinti, 2000](#)); iii) an oceanic plateau ([Pirajno, 2004](#)); iv) an intracontinental rift setting
56 ([Olieroor et al., 2018](#)).

57 In Africa, the UB series have been recognized in the Paleoproterozoic series of the southern
58 part of the West African Craton (WAC), which is structured in two separated domains
59 ([Bessoles, 1977](#)): (i) the Man rise, encompassing the Archean formations of the Liberia nucleus
60 (3.5 - 2.7 Ga) and the Paleoproterozoic (Birimian \approx 2 - 2.5 Ga) formations of the Baoulé-Mossi
61 domain; and (ii) the NW Birimian Kedougou and Kayes inliers ([Fig. 1](#)). In the WAC, the
62 Birimian formations of the Baoulé-Mossi and Kedougou-Kayes domains display two
63 petrographical and geochemical suites ([Bessoles, 1977](#)): (i) a magmatic UB-B suite (UB,
64 gabbros, basalts) of tholeiitic affinity; (ii) an ultramafic-mafic to differentiated suite (UB,
65 gabbro, granitoids, basalt, andesite, dacite, rhyolite) of calc-alkaline affinity.

66 Although volcanic series and granitoids have been a subject of a very large number of
67 studies (Doumbia et al., 1998; Gasquet et al., 2003; Dioh et al., 2006; Gueye et al., 2008;
68 Lambert-Smith et al., 2016; Parra-Avila et al., 2017), UB rocks have received little attention
69 despite being described throughout the WAC (Fig. 1): in the Katiola-Marabadiassa belt (Ivory
70 coast; Pouclet et al., 2006) (Fig. 1, zone 1), in the Ashanti belt (Ghana; Loh and Hirdes, 1999;
71 Attoh et al., 2006; Dampare et al., 2019 (Fig. 1, zone 2), in the Boromo belt (Burkina Faso;
72 Béziat et al., 2000; Castaing et al., 2003) (Fig. 1, zone 3), in the Kadiolo belt (Mali; Sangaré,
73 2008) (Fig. 1, zone 4), but especially in the Mako region (Eastern Senegal; Bassot, 1966; Dia,
74 1988; Ngom, 1995; Ngom et al., 1998 and 2010; Cissokho, 2010; Dabo et al., 2017; Fig. 1,
75 zone 5).

76 All the WAC UB occurrences have common characteristics, including forming slices
77 tectonically emplaced within the basic series as well as ranging in petrographic compositions
78 from dunites through to lherzolites, harzburgites and wehrlites. The proposed geodynamic
79 context associated with the UB rocks of the WAC remain controversial. According to the
80 published studies, the UB rocks are either interpreted as the cumulates associated with tholeiitic
81 volcanics (Ouédraogo, 1985; Dia, 1988; Ngom, 1995; Ngom et al., 1998; Pouclet et al., 2006;
82 Sangaré, 2008; Ngom et al., 2010; Cissokho, 2010; Dabo et al., 2017), as being genetically
83 related to the calc-alkaline series (Béziat et al., 2000) or as the testimony of a ophiolitic supra-
84 subduction environment (Attoh et al. 2006; Dabo et al. 2017; Dampare et al. 2019).

85 In the Mako area in eastern Senegal, UB rocks are often mentioned as presenting tholeiitic
86 affinity. However, some divergences may exist in the definition of the magmatic geodynamic
87 context. Indeed, UB lithologies in Mako would be related to: i) the lower unit of a lithospheric
88 fragment of the Birimian oceanic crust (ophiolite-like) with a marked tholeiitic affinity (OIB or
89 N-MORB, Dabo et al., 2017); or interpreted as ii) cumulates from a basaltic and gabbroic
90 tholeiitic melt, either N-MORBs or oceanic plateau basalts (Ngom, 1995; Ngom et al., 1998
91 and 2010; Cissokho, 2010). In the Loraboué massif of Burkina Faso UB rocks are interpreted
92 to have developed in conjunction with calc-alkaline series within an arc context (Béziat et al.,
93 2000).

94 This study presents new petrographic, mineralogical, geochemical (whole rock and in-situ
95 mineral major and trace elements) and isotopic data on UB rocks from the Mako and Loraboué
96 areas. The results of these analyses are then compared in order to discuss the geodynamic
97 context in which the UB occurrences within the WAC may have developed.

98 **2. Geological context**

99 **2.1. Kedougou - Kenieba Inlier**

100 The Birimian Kedougou - Kenieba Inlier (KKI) ([Fig. 2](#)) located in eastern Senegal and
101 western Mali is bounded on its western part by the Hercynian Mauritanides and unconformably
102 overlain by Neoproterozoic sediments of the Taoudenit basin ([Bassot, 1966](#)). The
103 Paleoproterozoic formations of the KKI are classically outcropping? within two series trending
104 NNE-SSW: the western series of the Mako greenstone belt and the eastern series of the Diale-
105 Dalema basin ([Bassot, 1966](#)). Towards the east, the Diale-Dalema is subdivided into the Faleme
106 Volcanic belt and the Kofi basin ([Lawrence, 2010; Lawrence et al., 2013; Lambert-Smith et al.,](#)
107 [2016; Masurel et al., 2017](#)). During the Eburnean orogeny (≈ 2.0 Ga, [Bonhomme, 1962](#)), the
108 KKI have encompassed polycyclic deformation phases and a widespread low-pressure
109 greenschist metamorphism, except the surrounding zone of the granitic plutons where
110 metamorphic conditions reach amphibolite facies ([Bassot, 1966; Masurel et al., 2017](#)).

111 The boundary between the western series of the Mako belt and the eastern series of the
112 Diale-Dalema is tectonic and marked by a regional fault system, 20 to 30 km wide striking
113 NNE-SSW ([Fig. 2](#)) and called by [Ledru et al. \(1989\)](#) the “Main Transcurrent Zone” (MTZ) (see
114 also [Gueye et al., 2007 and 2008; Théveniaut et al., 2010](#)). In this area, the series are strongly
115 deformed, leading to the disorientation of the original pattern, and locally to a juxtaposition of
116 tholeiitic and calc-alkaline magmatic, suites, like those described in Ghana by [Sylvester and](#)
117 [Attoh, \(1992\)](#) and in Burkina Faso by [Béziat et al. \(2000\)](#). The UB occurrences are located in
118 this high strain zone (MTZ) around the Mako village.

119 **2.2. Geology of the Mako area**

120 The Mako Belt have been the subject of numerous studies ([Bassot, 1966; Diallo, 1983;](#)
121 [Debat et al., 1984; Ngom, 1985; Dioh, 1986; Dia, 1988; Ngom, 1989; Abouchami et al., 1990;](#)
122 [Dioh et al., 1990; Boher et al., 1992; Diallo, 1994; Dioh, 1995; Ngom, 1995; Ngom et al., 1998;](#)
123 [Dioh et al., 2006; Pawlig et al., 2006; Gueye et al., 2007; Ngom et al., 2007; Gueye et al., 2008;](#)
124 [Ngom et al., 2010; Cissokho, 2010; Théveniaut et al., 2010; Ngom et al., 2011; Gozo et al.,](#)
125 [2015; Dabo et al., 2017; Gozo, 2017](#)). Magmatic series occur within the MTZ and consist of:
126 (i) a thick sequence of basalts locally pillowved as well as gabbro of tholeiitic affinity
127 interlayered with immature detrital sediments; ii) ultramafic rocks occurring as scattered slices,
128 associated with the tholeiitic suite; iii) basalt, andesite, dacite, rhyolite and gabbro defining a
129 more or less differentiated sequence with calc-alkaline affinity; these lithologies occur as veins

130 cross cutting the tholeiitic rocks. Series are intruded by amphibole-bearing granitoids of the
131 Badon-Kakadian Batholith and of smaller plutons (Tinkoto, Makana, Niemenike, Badon,
132 Soukouta (Bassot, 1966; Debat et al., 1984; Dioh et al., 2006; Gueye et al., 2008) (Fig. 2).

133 **3. Sampling and field observations**

134 We carried out a selective sampling trying to retrieve all sample types from all localities:
135 from the Mako village to Sofia prospect, located North-East of the Mako belt (Fig. 3a). Cross-
136 sections were done on each outcrop in order to collect samples from all the available lithological
137 types. Their GPS positions are available in Table 6.

138 In the Mako village area, the ultrabasic (UB) rocks occur as hectometric to plurikilometric
139 slices emplaced within the basalts, the gabbros and the metasediments. The major UB bodies
140 are: i) the western Mako UB massif (slice 1, Fig. 3b) trending NW-SE constituted only of
141 wehrlites (*IL18, IL32, MKNT312, MKNT313*); ii) the southeastern Mako UB massif trending
142 NNE-SSW and constituted of a slice of lherzolite (*ILL4*) (slice 2, Fig. 3b) and a slice of wehrlite
143 (*ILL3, 77*) (slice 3, Fig. 3b); iii) the Lame UB massif (slice 4, Fig. 3b) trending EW, 4 km long,
144 500 m wide. The Lame massif is petrographically composite and consists of lherzolite ($\approx 75\%$
145 of the volume) (*IL10, IL12, 53, ILL5, 125A, 128*) that includes metric to decametric
146 orthopyroxene-rich layers giving to the rock a harzburgitic composition (*IL51*). Near the
147 Koulountou village, 14 km Northeastern of Mako, two UB slices consisting of wehrlite (*116*)
148 (slice 5, Fig. 3c) and lherzolite (*IL9, 107*) (slice 6, Fig. 3c) occur, trending NNE-SSW (4 km
149 long and 1.2 km wide). Finally, in the Sofia area, a lherzolite (*132*) crops out (2 km long and
150 700 m wide), trending NNE-SSW (slice 7, Fig 3c).

151 **4. Sample processing and analytical methods**

152 16 samples from Mako village area have been selected for the geochemical study according
153 to petrographic criteria: 10 lherzolites, 1 harzburgite and 5 wehrlites. The mineral chemical
154 analyses were carried out using a Cameca SX Five electronic microprobe (Raimond Castaing,
155 University Toulouse III-Paul Sabatier). The analysis conditions were 15kV for the acceleration
156 voltage, for currents of 10 or 20 nA depending on the resistance of the minerals to the electron
157 beam. The acquisition times are 10 seconds at the peak and 5 seconds at either side of the peak
158 for the continuous background. The standards used for the measurement of concentrations are
159 natural or synthetic minerals as well as pure metals.

160 Samples dispatched for geochemical analysis were crushed and powdered in an agate
161 mortar, and dissolved in the GET Clean Lab according to the protocol described by [Yokoyama](#)
162 [et al. \(1999\)](#), modified by [Rospabé et al. \(2018\)](#). On another side, major element concentrations
163 have been obtained by X-ray fluorescence spectrometry (XRF) at Analytical Facility Centers:
164 Stellenbosch University (South Africa) and ALS (Spain). The trace element concentrations and
165 Sr/Nd isotopic measurements were performed at the Geosciences Environnement Toulouse
166 (GET) laboratory (Observatoire Midi-Pyrénées (OMP), University Toulouse III Paul Sabatier
167 (France)). Sample trace element concentrations were determined using an ELEMENT XR
168 (Thermo Scientific) High Resolution Inductively Coupled Plasma Mass Spectrometer (HR-
169 ICP-MS). Analytical geostandards and blanks were inserted within the sample sequence, and
170 the concentrations calculated according to the protocol described in [Rospabé et al. \(2018\)](#).

171 Mineral trace elements analyses were conducted with a Thermo Scientific HR-ICPMS
172 Element XR machine coupled to a New Wave Research NWR213 Nd YAG 213 nm laser
173 ablation unit. The counting time for one analysis was typically 210 s (60 s on gas blank to
174 establish background then 120 s for data collection followed by 30 s washout). The diameter of
175 the laser beam was around 40-50 µm, the frequency 7 Hz, and 4-5 J/cm² of laser fluency. A
176 maximum of 10 unknowns were bracketed by the measurement of two external standards: as
177 primary one the NIST SRM 610 and as secondary the NIST SRM 612. The secondary standard
178 was analyzed as unknown allowing the checking process of the precision and accuracy of the
179 analysis during the session. The relative precision and accuracy for a laser analysis ranges from
180 1 to 10% for most of the elements, but for Nb and Ta they are close to 15 %. Theoretical
181 detection limits for each element are in the range of 10 to 60 ppb except for Sc and V (100 ppb),
182 Ti (2 ppm), and Ni and Cr (0.7 ppm). The data reduction was carried out with the Glitter
183 software ([Griffin, 2008](#)).

184 Rb/Sr and Sm/Nd isotopic measurements were conducted on a MAT261 and Triton+
185 TIMS (OMP-GET, Toulouse). Before being measured, Sr and Nd have been purified in a
186 clean lab following the protocol described by [Pin et al. \(1994\)](#), and clean elemental fractions
187 of Sr and Nd were loaded respectively on W with Ta coating and Re filaments. Isotopic
188 standards NBS 987 for Sr and La Jolla for Nd give 0.710274 ± 4 and 0.511842 ± 2
189 respectively. Typical procedure blanks are 150 ng for Sr and 24 ng for Nd.

190 **5. Petrography and mineralogy**

191 Lherzolites ([Figs 4a and b](#)) present a heteradcumulate texture with associated cumulate
192 minerals (chromite ~ 3%, olivine ~ 50%) and intercumulus clinopyroxene (35 - 40%),
193 orthopyroxene (~ 10%), amphibole (2%) and phlogopite (1%). Olivine (Fo₇₈₋₈₅) crystals with
194 rounded to sub-rounded shape of variable size (0.03 - 0.9 mm) are often included in
195 clinopyroxene and orthopyroxene. Olivines are altered in serpentine and magnetite, which
196 occupy the peripheries and cracks of the crystals. Clinopyroxene (1.1 - 1.2 mm) is of augite
197 type (Wo₃₄₋₄₂, En₄₈₋₅₇, Fs₅₋₁₀; X_{Mg} = 0.9 - 0.8) and orthopyroxene has enstatite composition
198 (Wo₁₋₅, En₇₈₋₈₄, Fs₁₄₋₁₉; X_{Mg} = 0.9 - 0.8) following [Morimoto et al. \(1988\)](#) ([Fig. 5a](#)).
199 Clinopyroxene and orthopyroxene form euhedral to anhedral poikilitic crystals. Large
200 orthopyroxenes (1.9 - 3 mm) may include crystals of olivine and clinopyroxene. The brown
201 amphiboles (0.2 - 0.3 mm) are of the pargasite type (Si = 6.4 - 6.1 p.f.u.; X_{Mg} = 0.9 - 0.8) with
202 rare tschermakite composition (Si = 6.3 p.f.u.; X_{Mg} = 0.9) following the [Leake classification](#)
203 ([2003](#)) ([Fig. 5b](#)). They are found at interstitial position, between the grains of pyroxenes and
204 sometimes around olivine crystals. Phlogopite (X_{Mg} = 0.8) is also interstitial and appears as
205 small lamellae (0.06 - 0.1 mm). In the south of the Lamé massif (slice 4, [Fig.3b](#)), lherzolites
206 (*IL12, 55*) have a porphyritic texture ([Fig. 4c](#)), characterized by an increase of the
207 orthopyroxene crystal mode and size (0.5 - 1cm). This facies is composed of olivine (less
208 magnesian, Fo₇₅₋₇₇) and orthopyroxene of more ferriferous enstatitic composition (Wo₁₋₄,
209 En₇₇₋₇₈, Fs₁₉₋₂₁; X_{Mg} = 0.8).

210 Harzburgites (*IL51*) ([Fig. 4d](#)) have a heteradcumulate texture. Their mineralogy
211 consists of chromite (4%) plus olivine (53%) in cumulus position and intercumulus
212 orthopyroxene (41%) plus amphibole (2%). Euhedral to subhedral olivines (Fo₇₉₋₈₁) are of
213 variable size (0.3 - 0.5 mm) encompassed by the poikilitic orthopyroxenes. Orthopyroxenes
214 with enstatite composition (Wo₁₋₃, En₈₀₋₈₂, Fs₁₆₋₁₈; X_{Mg} = 0.8) form poikilitic xenomorphic
215 crystals (1.3 - 2 mm). The amphiboles (0.2 - 1 mm) are of edenite type (Si = 6.7 p.f.u.; X_{Mg} =
216 0.89) and of magnesio-hornblende type (Si = 7.2 - 6.5 p.f.u.; X_{Mg} = 0.9). They are interstitial
217 between the poikilitic crystals, including partially altered euhedral olivine crystals.

218 Wehrlites ([Fig. 4e](#)) present a heteradcumulate texture with chromite (3 - 4.5%), olivine
219 (64 - 73%), clinopyroxene (22.5 - 26%), amphibole (3%) and phlogopite (1%). Cumulus
220 olivine crystals (Fo₈₅₋₈₂) are euhedral to subhedral (0.03 - 1.3 mm), and display a rounded or
221 prismatic shape. They are altered in serpentine and magnetite. Clinopyroxene is of augite
222 composition (Wo₃₁₋₄₁, En₅₃₋₅₉, Fs₆₋₁₁; X_{Mg} = 0.9) with some rare intercumulus diopside (Wo₄₇₋
223 48, En₅₀₋₅₁, Fs₁₋₃; X_{Mg} = 1). Amphiboles (0.2 - 0.7 mm) are of pargasitic composition (Si = 6.4

224 p.f.u.; $X_{Mg} = 0.8$), interstitial between clinopyroxenes. Rare, small, interstitial lamellae of
225 phlogopite (1%) ($X_{Mg} = 0.9 - 0.8$) are found and typically the cleavages are underline by
226 opaque minerals. Some wehrlites crop out north-west of Lame (ILL3, 77) (Fig. 4f) are
227 distinguished by the occurrence of more magnesian olivine (Fo86-85), enstatitic
228 orthopyroxene (3 - 4%, Wo₁₋₃, En_{83 - 85}, Fs_{13 - 15}; $X_{Mg} = 0.9$) and pargasitic, interstitial
229 amphibole (2.5 - 4%, Si = 6.4 - 6.3 p.f.u.; $X_{Mg} = 0.8$), and sometimes rare edenite (Si = 6.5
230 p.f.u.; $X_{Mg} = 0.8$).

231 Lherzolites, harzburgites and wehrlites display the same primary and secondary oxide
232 minerals, but in different proportions (1 to 5%). Three types may be identified (Fig. 5c): i)
233 small, euhedral crystals of chromite ($X_{Mg} (Mg / Mg + Fe^{2+} + Ni + Mn) = 0.5 - 0.2$; $X_{Cr} (Cr / Cr$
234 + Al + Fe³⁺) = 0.6 - 0.5) of 0.001 - 0.004 mm in size are found as inclusions in olivine and
235 pyroxene crystals, consistent with their early crystallization; ii) Subhedral Cr-magnetite ($X_{Mg} =$
236 0.4 - 0.1; $X_{Cr} = 0.5 - 0.1$) as large crystals (0.02 - 0.05 mm) isolated or enclosed in pyroxene,
237 amphibole, phlogopite and in interstitial position. Given their textural position and their Cr-
238 magnetite composition (Kimball, 1990; Béziat et al., 2000), the Cr-magnetite may come from
239 ancient chromite crystals ; iii) anhedral magnetite crystals ($X_{Mg} = 0.1 - 0$; $X_{Cr} = 0$) as tiny
240 crystals (0.001 - 0.002 mm), often associated with serpentine and chlorite, filling veinlets,
241 olivine cracks and pyroxene, amphibole and phlogopite cleavages, are common
242 serpentinization by-products.

243 **6. Petrological and geochemical data**

244 LILEs (Large Ion Lithophile Elements) (Rb, Cs, Ba, Sr) are very sensitive to secondary
245 processes like low-grade metamorphism or water-rock interactions, while HFSE (High Field
246 Strength Elements) are little affected (Pearce et Cann, 1973; Winchester et Floyd, 1976; Condie
247 et al., 1977; Wood et al., 1979). Therefore, only samples with LOI under 10% will be discussed
248 in this section. However, their geochemical characteristics will be discussed according to their
249 petrological compositions.

250 **6.1. Major and minor elements (Fig. 6)**

251 Lherzolites have typical SiO₂ contents between 38.7% and 44.6%, which correlate
252 negatively with MgO and FeO. They present the lowest MgO and FeO(t) contents of our sample
253 set, as low as 13.3% and 10.6% respectively. Their FeO(t) are similar to that of wehrlites. Their
254 SiO₂ contents display a weak correlation with TiO₂ (and Al₂O₃), despite having the highest
255 TiO₂ content of all reported Birimian UB lithologies. Na₂O, K₂O, P₂O₅ and MnO do not show

any correlations with SiO₂, whereas CaO does. It is worth noting that some lherzolites display high CaO (up to 10%).

The only sampled harzburgite has a composition which falls globally within the reported WAC Birimian lithologies, having SiO₂ = 38.8% and MgO = 30.7%. However, this sample displays the highest FeO(t) content (FeO(t) = 15.4%) of our sample set, similar to those reported for Bouroum Yalogo lherzolites ([Ouédraogo, 1985](#)). TiO₂ (0.3%) and Al₂O₃ (3.48%) are within what is expected for this lithology.

The wehrellites present a relatively large range of SiO₂, between 38.3% and 41.5% and high MgO contents, up to 35%, associated with low FeO(t) (as low as 10.6%). In the Harker diagrams ([Fig. 6](#)), they do not fall systematically within the field of the reported wehrellites from the literature, sharing some major element characteristics with Mako wehrellites ([Ngom et al., 2010](#)) for MgO, TiO₂ and Al₂O₃, but having lower FeO(t) contents, similar to those reported in Loraboué ([Béziat et al., 2000](#)). In terms of correlations, SiO₂ shows a negative correlation with MgO, and positive correlation with TiO₂, CaO and Al₂O₃. One of our analyzed samples presents a relatively high K₂O (0.3%). Their Ni contents vary from 1670 to 3002 ppm and Cr from 2268 to 2721 ppm. It is worth noting that Opx-wehrellites have higher SiO₂, CaO contents and lower MgO, Cr₂O₃, X_{Mg} and Ni contents than wehrellites without orthopyroxene.

6.2. Trace elements

6.2.1. Lherzolites and harzburgites

Whole rocks

Lherzolites are moderately depleted in Rare Earth Elements (REE) ($\sum\text{REE} = 35$ to 113 ppm), from 2 to 7 times chondrites (Ch.) for LREE (Light REE) and 2 to 5 times Ch. for HREE (Heavy REE). They are characterized by convex patterns with moderate La_N/Yb_N = 1 - 1.6, almost flat La_N/Nd_N (0.8 - 1) and fractionated (Dy_N/Lu_N = 1.5 - 1.7) ([Fig. 7a](#)). All but one of the lherzolite analyzed display a negative Eu anomaly (Eu/Eu* = 0.8 - 1). One of the lherzolite (sample 107) is characterized by a lower amount of REE, about 2 times less than the other samples, and no negative Eu anomaly. The harzburgite sample is characterized by a $\sum\text{REE} = 70$ ppm and has a less convex REE pattern, with flat LREE (La_N/Nd_N = 1.1), MREE (Middle REE) (Sm_N/Gd_N = 1) and still fractionated HREE (Dy_N/Lu_N = 1.5), with no Eu anomaly (Eu/Eu* = 1).

286 On extended trace element normalized diagrams, the lherzolites display patterns flat to
287 slightly depleted in the most incompatible elements. They lie systematically above the primitive
288 mantle, far from any residual mantle typical composition ([Sun and McDonough, 1989](#)) ([Fig.](#)
289 [7b](#)). The lherzolite patterns are also characterized by systematic negative Th, Nb and Zr,
290 positive Rb, Ba, and positive to negative Pb, Sr and Ti anomalies. The anomalously low
291 lherzolite pattern is characterized by the absence of Nb, Pb and Th anomalies and display
292 negative Sr and Zr and positive Ti anomalies. The harzburgite extended pattern is close to the
293 lherzolites with positive Rb, U and negative Nb, Pb and Ti anomalies.

294 **Clinopyroxenes**

295 Lherzolite clinopyroxene trace element contents have been determined for *IL10*, *ILL4*
296 and *136* samples. In *IL10* lherzolite, clinopyroxenes plot as two distinct populations,
297 characterized by their parallel LREE patterns but having different Eu anomaly ([Fig. 7c](#)). The
298 first population is depleted in REE (Σ REE = 53 to 75 ppm), and displays a global convex
299 pattern, with LREE of 1 to 2 times Ch. ($\text{La}_N/\text{Nd}_N = 0.4$) and slightly depleted HREE (Dy_N/Lu_N
300 = 1.2 - 1.3). For this population, the europium shows very weak negative anomalies ($\text{Eu}/\text{Eu}^* = 0.9$).
301 The second population, which has higher REE content (Σ REE = 124 to 131 ppm) also
302 displays convex pattern, with a marked depletion in LREE ($\text{La}_N/\text{Nd}_N = 0.4 - 0.5$), HREE
303 ($\text{Dy}_N/\text{Lu}_N = 1.7 - 1.8$) and systematic negative anomalies in europium ($\text{Eu}/\text{Eu}^* = 0.6 - 0.7$). In
304 *ILL4* lherzolite, the clinopyroxenes patterns are different than those of the *IL10* lherzolite.
305 Clinopyroxenes of *ILL4* lherzolite are characterized by a slight LREE depletion (5 to 6 times
306 Ch. ($\text{La}_N/\text{Nd}_N = 0.7 - 0.8$), slight enrichments in MREE ($\text{Sm}_N/\text{Tb}_N = 0.9$) and flat HREE. The
307 clinopyroxene of the sample *136* of lherzolite has the most LREE depleted pattern ($\text{La}_N/\text{Nd}_N = 0.3 - 0.4$),
308 systematic negative anomalies in Eu ($\text{Eu} / \text{Eu}^* = 0.9$), and a relative depletion in
309 HREEs ($\text{Dy}_N/\text{Lu}_N = 1.7 - 2.4$). In extended diagram ([Sun and McDonough, 1989](#)) ([Fig. 7d](#)), the
310 most incompatible elements are below or close to the detection limit for clinopyroxene. *IL10*,
311 *ILL4* and *136* lherzolite clinopyroxenes show negative Nb, Pb, Sr, Zr and Ti and positive Th,
312 Y anomalies, except for the clinopyroxenes of the first population of the *IL10* lherzolite, which
313 have negative Th anomalies and sample *136* which has positive Pb anomalies.

314

315 **Amphiboles**

316 The only amphibole trace element data have been obtained for lherzolite *ILL4*. In terms
317 of trace element contents, amphibole is characterized by enrichment in REE (Σ REE = 811 -
318 1161 ppm), a general fractionation from LREE ($\text{La}_N/\text{Nd}_N = 1.3 - 1.7$) to HREE ($\text{Dy}_N/\text{Lu}_N = 1.2$
319 - 1.3) and almost no Eu anomalies (Fig. 7c). Regarding the other trace elements, the amphiboles
320 are characterized by marked negative Rb, U, Pb and Sr anomalies. Like for REE, the other trace
321 elements are enriched (10 to 100 times), comparatively to the clinopyroxenes in the same
322 sample (Fig. 7d).

323 **6.2.2. Wehrlites**

324 Whole rocks

325 Wehrlites have the most enriched REE and trace element contents of all the sample set.
326 They have rather similar REE patterns (Σ REE = 45 to 119 ppm), homogeneously fractionated
327 ($\text{La}_N/\text{Yb}_N = 2 - 2.5$). They are characterized by weak negative Eu anomalies ($\text{Eu}/\text{Eu}^* = 0.9$). In
328 comparison to the other ultrabasic samples, they are systematically enriched in LREE but have
329 same range of HREE (Fig. 7e). In extended normalized trace element diagrams (Fig. 7f),
330 wehrlites are characterized by Nb, Sr and in lesser extent Ti negative anomalies, positive
331 anomalies in Ba, U and positive to negative Pb anomalies. Like for lherzolites, they fall above
332 the Primitive Mantle values, being therefore enriched in comparison to normal residual upper
333 mantle, depleted or not.

334 Clinopyroxenes

335 The *116* wehrlite clinopyroxene display moderately enriched REE content (Σ REE = 46)
336 with an almost flat pattern, slightly depleted in HREE ($\text{Dy}_N/\text{Lu}_N = 1.4$), without significant Eu
337 anomaly. In terms of REE, the pattern is very close to the whole rock, being less enriched in
338 LREE. On the other side, orthopyroxene-wehrlite clinopyroxenes (*ILL3*) are characterized by
339 their depletion in LREE ($\text{La}_N/\text{Nd}_N = 0.3 - 0.5$) compared to HREE ($\text{Dy}_N/\text{Lu}_N = 1.2 - 1.8$), being
340 globally more enriched in REE than sample *116* clinopyroxene. Europium display weak
341 negative anomalies ($\text{Eu}/\text{Eu}^* = 0.9$) and the patterns are more consistent with what is expected
342 from clinopyroxenes in equilibrium with a basaltic melt (Fig. 7g). On extended diagrams (Fig.
343 7h), apart from the elements that fall below the detection limit, the clinopyroxene (for both
344 wehrlites) display negative U, Th, Nb, Pb, Sr, Zr and Ti anomalies except for sample *ILL3*
345 which has no Ti anomaly. The main differences between the two populations of clinopyroxene
346 are the level of trace element, which are lower for sample *116* clinopyroxene.

347 Amphiboles

348 Trace element contents have been determined for amphibole in sample *116*. In this
349 sample, amphibole is characterized by their high REE contents ($\Sigma\text{REE} = 1557 - 1705 \text{ ppm}$) and
350 fractionated REE patterns. The patterns are almost parallel to those of amphibole in lherzolite
351 *ILL4*, being globally more enriched and displaying systematic negative europium anomaly
352 ($\text{Eu/Eu}^* = 0.5$) (Fig. 7g). Like for *ILL4* (lherzolite) amphiboles, extended trace element patterns
353 display marked negative Rb, U, Pb, Sr more Th and Ti anomalies (Fig. 7h).

354 **6.2.3. New data for Loraboué wehrlites**

355 Loraboué wehrlites display whole rock REE normalized patterns different from those
356 of Mako, being convex, more depleted, and with a flat MREE to HREE shape ($\Sigma\text{REE} = 32 -$
357 87 ppm, $\text{La}_N/\text{Nd}_N = 1.8 - 1.9$; $\text{Sm}_N/\text{Gd}_N = 1.1 - 1.2$; $\text{Dy}_N/\text{Lu}_N = 0.9 - 1$). Comparatively,
358 clinopyroxene and amphibole REE patterns fall systematically above the whole rock. The
359 clinopyroxene have a marked convex pattern, with high La_N/Nd_N and low Gd_N/Lu_N ratios and
360 weak Eu negative anomalies. Amphiboles, on the opposite, display concave REE patterns, with
361 marked negative Eu anomalies. They are characterized by LREE depletion, and a REE pattern
362 shape very close to those of lherzolite clinopyroxenes, while being 10x more enriched (Fig. 7i).
363 In extended trace element diagrams, whole rocks are characterized by negative Nb, Sr, Ti and
364 positive Pb, Zr anomalies. Clinopyroxene display negative Ba, Nb, Sr and Ti and positive Th,
365 U anomalies while amphiboles have negative Th, U, Pb, Sr, Zr, Ti and positive Ba anomalies
366 (Fig. 7j). It is worth noting that Loraboué wehrlite, both in terms of whole rock and mineral
367 trace element concentrations, display very different pattern profiles than the one found in Mako
368 for the same lithology.

369 **6.2.4. Comparison between whole rock, clinopyroxene and amphibole trace
370 element data**

371 When reported one lherzolite (*ILL4*) and wehrlite (*116*) samples from Mako and a
372 wehrlite (*Lo113*) sample from Loraboué in a $\text{Sm}_{\text{PM}}/\text{Yb}_{\text{PM}}$ vs $\text{Nb}_{\text{PM}}/\text{La}_{\text{PM}}$ diagram (Fig. 8), Mako
373 and Loraboué UB show distinctive features. It is worth mentioning that for all samples the WR
374 (whole rock) composition falls between the clinopyroxene and amphibole composition fields,
375 showing a linear correlation for Mako village area samples and hyperbolic correlation for
376 Loraboué. This is suggesting that the trace element signatures for the WR are almost entirely
377 controlled by these two minerals, but differently for the two localities. The fact that the

378 Loraboué wehrlite is not showing the same type of correlation may be either related to the
379 relative abundance of Nb, La, Sm, and Yb in both minerals in this sample or to another mineral
380 carrying sufficient trace elements to influence the mixing curve. Such mineral may be
381 orthopyroxene or phlogopite; however these minerals are also present in Mako wehrlite. The
382 other reason may be the relatively low Nb content in clinopyroxene for Loraboué wehrlite,
383 which may influence the curvature of the mixing line.

384 **7. Nd and Sr isotopic signatures**

385 Sr and Nd isotopic ratios have been determined for 14 ultramafic samples, respectively
386 5 wehrlites, 8 lherzolites, and 1 harzburgite. Lherzolite samples are characterized by $^{87}\text{Sr}/^{86}\text{Sr}$
387 (2.1 Ga) between 0.703294 and 0.708842 and $^{143}\text{Nd}/^{144}\text{Nd}$ (2.1 Ga) between 0.512989 and
388 0.513167, wehrlite having $^{87}\text{Sr}/^{86}\text{Sr}$ (2.1 Ga) from 0.711904 to 0.719083 and $^{143}\text{Nd}/^{144}\text{Nd}$ (2.1
389 Ga) between 0.512509 and 0.512643 and the harzburgite sample has a $^{87}\text{Sr}/^{86}\text{Sr}$ (2.1 Ga) of
390 0.703125 and a $^{143}\text{Nd}/^{144}\text{Nd}$ (2.1 Ga) of 0.512792. Reported in isochron diagrams ([Fig 9a](#) and
391 b), we can observe that their isotopic ratios are globally proportional to their Father/Daughter
392 ratios, both for Sm/Nd and Rb/Sr, and that they align along a c. 2.1 Ga calculated isochron. This
393 observation confirms that these samples are related to a Birimian magmatic episode, and not
394 disconnected from the whole Mako magmatism ([Abouchami et al., 1990](#); [Boher et al., 1992](#);
395 [Pawlig et al., 2006](#); [Ngom et al., 2010](#)). Note however that the data are not perfectly fitting the
396 calculated isochrons ([Fig 9a](#) and b). Powder heterogeneity problems can be excluded since both
397 concentration and isotopic compositions were measured on the same dissolution batch. Rb/Sr
398 isotopic chronometer is, however, known to be sensitive to metamorphism and may be more
399 easily perturbed leading to Rb/Sr isotopic data spread. Sm/Nd, on the other hand, is less
400 sensitive to metamorphic processes and display a similar data spread. According to these
401 observations, our data have been corrected from an age of c. 2.1 Ga in order to compare them
402 to the available Birimian data ([Fig. 9c](#)). In the Nd/Sr correlation diagram (2,1 Ga), our data are
403 comparable with published data for the WAC ([Abouchami et al., 1990](#); [Alric, 1990](#); [Boher et](#)
404 [al., 1992](#); [Ama Salah et al., 1996](#); [Dia et al., 1997](#); [Gasquet et al., 2003](#); [Pawlig et al., 2006](#);
405 [Dampare et al., 2009](#); [Ngom et al., 2010](#); [Dampare et al., 2019](#)). Nevertheless, as the dataset
406 does not define a single domain, our results imply either that the age corrections propagate large
407 uncertainties or that these lithologies do not share the same source. Both hypotheses will be
408 discussed below.

409 **8. Discussion**

410 **8.1. UB rocks from Mako.**

411 The UB rocks identified in Mako consist of lherzolite / harzburgite, wehrlite or
412 lherzolite / wehrlite petrographic associations massifs. These UB rocks have a similar
413 cumulative texture and mineralogical composition. The only difference is the occurrence of
414 orthopyroxene, which is still present in lherzolites and harzburgites, and absent in isolated
415 wehrlite massifs (wehrlite (*ILL3*) excepted). The cumulative texture of these rocks, the mineral
416 chemical composition (olivine with a Fo at % < 90%, Augite-type and non-Cr-diopside-type
417 clinopyroxene, chromite-type and non-Mg-spinel type) and their trace element contents are
418 systematically higher than that of the primitive mantle. This in turn indicates that these UB
419 rocks represent ultramafic cumulates that cannot be confounded with peridotites from the upper
420 mantle.

421 The two types of UB rocks intercalated in the tholeiitic sequence in Mako exhibit
422 mineral compositions showing that wehrlite present magnesian-rich clinopyroxenes and
423 chromium rich chromites when compared to both clinopyroxenes and chromites from the
424 lherzolite and harzburgite. Similarly the whole rock compositions are fractionated for wehrlite
425 ($\text{La}_\text{N}/\text{Yb}_\text{N} > 2$) and flat to slightly fractionated for lherzolite / harzburgite ($\text{La}_\text{N}/\text{Yb}_\text{N} = 1 - 1.5$).
426 These differences are also found in the compositions of mineral compositions acquired on
427 clinopyroxenes. Clinopyroxenes analysed in the lherzolite / harzburgite and wehrlite / lherzolite
428 association show convex shaped spectra, low in both LREE and HREE with a clear negative
429 anomaly in Eu, whereas clinopyroxenes analysed in the wehrlite are clearly enriched in LREE
430 and do not show negative Eu anomalies.

431 Both whole rock and mineral composition differences indicate that the UB rocks in
432 Mako may derive from two distinctive parent magmas. As regards the wehrlite type, there are
433 in fact two distinct types of wehrlite in Mako: 1) the first, more rarely observed, is associated
434 with the lherzolites; 2) the second, most common, is found as isolated massifs. This result
435 differs from that of previous studies that suggested that the UB rocks from Mako derived from
436 a single source ([Ngom et al., 1998 and 2010; Cissokho, 2010; Dabo et al., 2017](#)).

437 **8.2. Mako vs Loraboué**

438 Within the Loraboué district (Boromo greenstone belt), wehrlite is associated with
439 dunite that have been interpreted as cumulates within the calc-alkaline magmatic serie ([Béziat
440 et al., 2000](#)). Loraboué and Mako samples present similar petrography with a heteradcumulate

441 texture, cumulus chromite + olivine and intercumulus clinopyroxene + orthopyroxene +
442 amphibole + mica (phlogopite type at Mako, biotite type at Loraboué). They have comparable
443 major element composition with Loraboué wehrlite presenting lower TiO₂, FeO(t) and Cr
444 contents.

445 The Loraboué samples show distinctive whole rock REE patterns and mineral
446 compositions when compared to the Mako samples. REE patterns of Loraboué wehrlite are U-
447 shaped, whereas those of Mako wehrlite are fractioned, LREE enriched. In extended trace
448 element diagrams, Loraboué wehrlite samples show a clear negative Nb anomaly. Mineral
449 analyses also indicate that olivine from Loraboué present a more homogeneous Fo composition
450 when compared to the Mako wehrlites. In Loraboué wehrlites, chromite compositions present
451 lowest chromium concentrations ([Fig. 10a and b](#)) and the clinopyroxenes shows low SiO₂, MgO
452 and FeO(t) concentrations ([Fig. 10c and d](#)). Amphiboles of Loraboué of pargasite type are less
453 titaniferous and more aluminous than those of Mako sample suites ([Fig. 10e, f, g and h](#)). The
454 REE patterns of clinopyroxenes from Loraboué display a concave pattern that contrasts from
455 that of the Mako sample showing flat or convex patterns. Moreover, clinopyroxenes in
456 Loraboué show high Th and U contents and a strong negative Nb anomaly. Similarly,
457 amphiboles from the Loraboué samples show clear negative anomalies in Ti and Zr.

458 Using different REE ratios, Tb_N/Yb_N vs Lan/Sm_N ([Fig. 11](#)), one can clearly separate two
459 populations of UB rocks (whole rock and clinopyroxene compositions) within the Mako
460 complexes, and distinguish them from those of Loraboué. These differences in composition
461 would again reflect the differences in the composition of the parent magmas, of a tholeiitic
462 nature in Mako and of a more calc-alkaline composition in Loraboué. All these features suggest
463 that they belong to very different geodynamic settings.

464 **8.3. Mako-Loraboué vs WAC**

465 The comparison between the UB of Mako and Loraboué and the UB of the WAC is
466 difficult, data about the latter being rare and fragmented. The limited dataset shows that all UB
467 samples from the WAC share some characteristics with those of the Mako UB rocks including:
468 cumulate textures and petrographic associations (i.e. dunites, lherzolites, harzburgites and
469 wehrellites). The Mako UB rocks are comparable to those of the Katiola-Marabadiassa belt (Ivory
470 Coast, [Pouclet et al., 2006](#)) but stand out from the UB of the other WAC deposits, showing
471 higher Gd_N/Yb_N and lower Lan/Sm_N ratios ([Fig. 12](#)). These differences may reflect the nature
472 of the parent magma, tholeiitic for Mako and Katiola-Marabadiassa, calc-alkaline for Kadiolo

473 and Loraboué. It is worth mentioning that Ashanti UB (Ghana, [Dampare et al. 2019](#)) are
474 characterized by flat REE patterns, which explain why they fall in a distinctive quadrant in [Fig.](#)
475 [12](#): they have similar Lan/Smn that Mako harzburgites but lower Gd_N/Ybn. They may
476 correspond to an intermediate geodynamic context, i.e. in equilibrium with a more depleted
477 melt. This feature is also suggested by the very juvenile Nd and Sr isotopic signatures of the
478 Ashanti mafic (and in a lesser extend ultramafic) series ([Dampare et al. 2009 and 2019](#)).
479

8.4. Origin of the parental melts

480 The isotopic signatures of Mako UBs reported in the ϵ Nd (2.1 Ga) vs $^{87}\text{Sr}/^{86}\text{Sr}$ (2.1 Ga)
481 diagram ([Fig. 9](#)) do not allow to decipher between different geodynamic environments.
482 Compared to the available data ([Ngom et al., 2010; Dampare et al., 2019](#)), they are more scattered
483 but fall within a domain that is considered linked to c. 2.1 Ga depleted (to slightly enriched)
484 mantle ([Abouchami et al., 1990; Dia et al., 1997; Gueye et al., 2007](#)). However, the Mako UB
485 rocks display the most primitive isotopic signatures ever reported for Mako mafic rocks, and are
486 slightly more scattered than the signatures found in the associated mafic lithologies ([Abouchami](#)
487 [et al., 1990; Dia et al., 1997; Pawlig et al., 2006; Ngom et al., 2010](#)). Scattering of the
488 geochemical signatures within a single magmatic system, deeply rooted into the lithosphere, has
489 been already reported in UB from oceanic or ophiolitic settings ([Benoit et al., 1996; Koga et al.,](#)
490 [2001; Drouin et al., 2009; Nicolle et al., 2016](#)). Being cumulates from more primitive melts,
491 Mako UBs display more heterogeneous isotopic signatures than the more evolved, more mixed,
492 mafic occurrences, whether being genetically related or not. However, one cannot discard the
493 hypothesis that the scattering of the isotopic signatures comes from the age correction and
494 analytical uncertainties. The error propagation associated with age correction may be
495 dramatically enhanced if the father/daughter ratios have been changed during metamorphic
496 processes after the emplacement. In order to test this hypothesis, data have been reported in a
497 ϵ Nd (2.1 Ga) vs $\alpha(\text{Sm/Nd})$ diagram ([De Paolo and Wasserburg, 1976a, b; De Paolo, 1988](#)). This
498 representation ([Fig. 13](#)) is similar to the one used in [Dampare et al. \(2009\)](#) and [Roddaz et al.](#)
499 ([2007](#)), with the exception that zero-age mafic and ultramafic samples can be reported together
500 with c. 2.1 Ga old samples in a single diagram. Obviously, Birimian samples from the WAC do
501 not plot in the same quadrant as present-day MORBs and Oceanic Arc basalts (see [Fig. 11](#) for
502 references). However, they correlate with Mantle-Crust evolution lines. On this zero-age
503 evolution line, we can observe that moving from right to left the samples are more and more arc-
504 related with time. For modern ultramafic rocks, samples sitting at the right-hand side of the
505 horizontal axis are classically associated with Mid-Oceanic Ridge settings. A similar logic may

506 be applied to the Birimian samples. On Fig. 13 Mako lherzolites fall on the right-hand side of the
507 correlation line. Accordingly the Mako samples analysed may be considered as the most MORB-
508 related UB ever described within the WAC both showing elevated $\alpha(\text{Sm}/\text{Nd})$ and εNd (2.1 Ga)
509 (Fig. 13). In the same diagram (Fig. 13), the lherzolite/harzburgite association from Mako are
510 characterized by more juvenile signatures than the wehrlite found in isolated massifs, which tends
511 to have lower $\alpha(\text{Sm}/\text{Nd})$. This change in composition may be related to an arc-like source.
512 Collectively, we suggest that the Mako UB-rocks are related to two contrasting geodynamic
513 environments. The first one appears to be juvenile or mantle-related, as far as the trace elements
514 are concerned (Fig. 7, 12) whereas the second one is more arc-related. Such dichotomy (arc vs
515 ridge setting) in a single geological area is a common occurrence in the Oman ophiolite (Python
516 et al., 2003 and references therein). Alternatively, for some ophiolitic sequences, or supposed
517 ophiolitic sequences this dichotomy may highlight a tectonic overprint which juxtaposed blocks
518 that are not genetically related, like for example in the Trinity Ophiolite (Lanphere et al., 1968;
519 Jacobsen et al., 1984; Gruau et al., 1998; Ceuleneer and Le Sueur, 2008). In the absence of
520 obvious structural relations, we suggest that the wehrellites and lherzolites/harbzburgites associations
521 in Mako may belong to a single oceanic basin in which the setting has evolved from a MORB to
522 a subduction-related environment over a period beyond the precision of our measurements.

523 9. Conclusion

524 This study on Mako's UB associations emplaced within the basic tholeiitic series
525 (gabbros, basalts), revealed a duality of composition within the tholeiitic series. REE, trace
526 elements in whole rocks and mineral (essentially clinopyroxene and amphibole) and Nd
527 isotopes suggest that the two different types of complexes, lherzolite + harzburgite assemblages
528 and isolated wehrelite massifs, are settled in two different geodynamic environments, the
529 lherzolite-harzburgite association being significantly more juvenile than isolated wehrellites,
530 which show transitional geochemical signatures.

531 Conversely, Loraboué UB rocks (dunite + wehrlite), clearly associated with the calc-
532 alkaline series and displaying the same mineralogical composition as the Mako wehrellites are
533 characterized by evolved petrological and geochemical signatures, typically emplaced in
534 mature island-arc magmas.

535 Through the study of UB complexes, we have been able to highlight the importance of
536 enclosing the UB petrological and geochemical data in geodynamic reconstructions. These
537 lithologies reveal part of the magmatic heterogeneity within a same province, suggesting that

538 the Birimian crust was built in an oceanic context evolving from a MORB-like domain to an
539 increasingly mature volcanic arc domain.

540 **Acknowledgments**

541 Our research was co-financed by the West African Exploration (WAXI) project and the
542 Cultural Action Cooperation Service of the French Embassy in Senegal. We wish to gratefully
543 acknowledge AMIRA International and the industry sponsors for their support of the WAXI
544 project (P934B). We are also appreciative of the contribution of the various geological surveys
545 department of mines in West Africa as sponsors in kind of WAXI. We thank the Cultural Action
546 Cooperation Service which awarded the PhD co-tutelle fellowship for 12 months of stay in
547 France, with a financial support for analytical work. We also want to thank the mining
548 companies (Torogold Ltd., Randgold Resources) for hosting us during the fieldwork. Our
549 thanks also go to André Pouclet who sent us his data and Séta Naba who helped us to get some
550 bibliographic references. We would like to thank Fabienne De Parseval, Philippe De Parseval,
551 Sophie Gouy and Stéphanie Mounic for making thin sections and for their technical assistance
552 during the microprobe and TIMS analyzes.

553 **References**

- 554 Abouchami, W., Boher, M., Michard, A., Albarede, F., 1990. [A major 2.1 Ga old event of mafic](#)
555 [magmatism in West Africa: an early stage of crustal accretion](#). Geophys. Res. Lett. 95, pp.
556 [17605-17629](#).
- 557 Albarede, F., 1998. [The growth of continental crust](#). Tectonophysics 296, 1-14.
- 558 Ama-Salah, I., Liégeois, J., Pouclet, A., 1996. [Evolution d'un arc insulaire océanique birimien précoce](#)
559 [au Liptako nigérien \(Sirba\): géologie, géochronologie et géochimie](#). J. Afr. Sci. 22, 235-254.
- 560 Attoh, K., Evans, M.J., Bickford, M.E., 2006. [Geochemistry of an ultramafic-rodingite rock association](#)
561 [in the Paleoproterozoic Dixcove greenstone belt, southwestern Ghana](#). J. Afr. Earth Sci. 45, 333-
562 [346](#).
- 563 Barrat, I.A., Zanda, B., Jambon, A., Bollinger, C., 2014. [The lithophile trace elements in enstatite](#)
564 [chondrites](#). Geochim. Cosmochim. Acta 128, 71-94.
- 565 Bassot, J.P., 1966. [Etude géologique du Sénégal oriental et de ses confins Guinéo Maliens](#). Mémoire
566 [BRGM, N°. 40](#), 332 p.
- 567 Ben Othman, D., Polvé, M., Allègre, C.J., 1984. [Nd–Sr isotopic composition of granulites and](#)
568 [constraints on the evolution of the lower continental crust](#). Nature 307, 510-515.
- 569 Benoit, M., Polvé, M., Ceuleneer, G., 1996. [Trace element and isotopic characterization of mafic](#)
570 [cumulates in a fossil mantle diapir \(Oman ophiolite\)](#). Chem. Geol. 134, 199-214.
- 571 Bessoles, B., 1977. [Géologie de l'Afrique. Le craton ouest- africain](#). Mémoire BRGM, Paris. 88 p.

- 572 Béziat, D., Bourges, F., Debat, P., Lombo, M., Martin, F., Tollon, F., 2000. A Paleoproterozoic
573 ultramafic – mafic assemblage and associated volcanic rocks of the Boromo greenstone belt:
574 fractionates originating from island – arc volcanic activity in the West African Craton.
575 *Precambrian Res.* 101, 25-47.
- 576 Boher, M., Abouchami, W., Michard, A., Albarede, F., Arndt, N.T., 1992. *Crustal growth in West Africa*
577 at 2.1 Ga. *J. Geophys. Res.* 97, pp. 345-369.
- 578 Bonhomme, M., 1962. Contribution à l'étude géochronologique de la plate-forme de l'Ouest africain.
579 *Ann. Fac. Sci. N°. 5, Univ. Clermont-Ferrand.*
- 580 Burg, J.-P., Bodinier, J.-L., Gerya, T., Bedini, R.-M., Boudier, F., Dautria, J.-M., Prikhodko, V., Efimov,
581 A., Pupier, E., Balanec, J.-L., 2009. *Translithospheric Mantle Diapirism: Geological Evidence*
582 and Numerical Modelling of the Kondyor Zoned Ultramafic Complex (Russian Far-East). *J.*
583 *Petrol.* 50, 289-321.
- 584 Castaing, C., Billa, M., Milesi, J., Thiéblemont, D., Le Metour, J., Egal, E., Donzeau, M. (BRGM)
585 (coordinateurs), Guerrot, C., Cocherie, E.A., Chevremont, P., Tegyey, M., Itard, Y. (BRGM),
586 Zida, B., Ouédraogo, I., Koté, S., Kaboré, B.E., Ouédraogo, C. (BUMIGEB), Ki, J.C., Zunino,
587 C. (ANTEA), 2003. *Notice explicative de la Carte géologique et minière du Burkina Faso à 1/1*
588 *000 000.*
- 589 Ceuleneer, G., Le Sueur, E., 2008. The trinity ophiolite (California): the strange association of fertile.
590 *Bull. Soc. Géol. Fr.* 179, 503-518.
- 591 Cissokho, S., 2010. *Etude géologique du secteur de Mako (partie méridionale du super-groupe de Mako,*
592 *boutonnière de Kédougou-Kéniéba, Sénégal oriental): implications sur la diversité*
593 *magmatique.* Thèse de doctorat 3ème cycle Univ. Cheikh Anta Diop, Dakar, Sénégal. 212 p.
- 594 Condie, K.C., 2000. Episodic continental growth models: Afterthoughts and extensions. *Tectonophysics*
595 322, 153-162.
- 596 Condie, K.C., 1994. Archean crustal evolution In: Windley, B.F. (Ed.). *Dev. Precambrian Geol.* 528 p.
- 597 Condie, K.C., Viljoen, M. J., Kable, E.J.O., 1977. Effects of alteration on elements distributions in
598 *Archean tholeiites from the Barberton greenstones belt.* *South Afr. Contrib. Miner. Pet.* 64, 75-
599 89.
- 600 Dabo, M., Aïfa, T., Gning, I., Faye, M., Ba, M.F., Ngom, P.M., 2017. *Lithological architecture and*
601 *petrography of the Mako Birimian greenstone belt, Kédougou-Kéniéba Inlier, eastern Senegal.*
602 *J. Afr. Earth Sci.* 131, 128-144.
- 603 Dampare, S., Shibata, T., Asiedu, D., Okono, O., Manu, J., Sakyi, P., 2009. *Sr–Nd isotopic compositions*
604 *of Paleoproterozoic metavolcanic rocks from the southern Ashanti volcanic belt, Ghana.* *Earth*
605 *Sci. Rep.* 16, 9-28.
- 606 Dampare, S.B., Shibata, T., Asiedu, D.K., Okano, O., Osae, S.K.D., Atta-Peters, D., Sakyi, P.A., 2019.
607 *Ultramafic–mafic and granitoids supra-subduction magmatism in the southern Ashanti volcanic*
608 *belt, Ghana: Evidence from geochemistry and Nd isotopes.* *Geol. J.* 1-37.

- 609 Debat, P., Diallo, D.P., Ngom, P.M., Rollet, M., Seyler, M., 1984. *La série de Mako dans ses parties*
610 *centrale et méridionale (Sénégal Oriental, Afrique de l'ouest). Précisions sur l'évolution de la*
611 *série volcanosédimentaire et données géochimiques préliminaires sur les formations*
612 *magmatiques post-tectoniques.* J. Afr. Earth Sci. 2, 71-79.
- 613 DePaolo, D.J., 1988. *Neodymium Isotope Geochemistry, Minerals and Rocks.* Springer Berlin
614 Heidelberg.
- 615 DePaolo, D.J., Wasserburg, G.J., 1976. *Nd isotopic variations and petrogenetic models.* Geophys. Res.
616 Lett. 3, 249-252.
- 617 Dia, A., 1988. *Caractère et signification des complexes magmatiques et métamorphiques du secteur de*
618 *Sandikounda-Laminia (Nord de la boutonnière de Kédougou, Est du Sénégal): Un modèle*
619 *géodynamique du Birimien de l'Afrique de l'Ouest.* Thèse de doctorat d'état Univ. Cheikh Anta
620 Diop de Dakar, Sénégal. 350 p.
- 621 Dia, A., Van Schmus, W.R., Kröner, A., 1997. *Isotopic constraints on the age and formation of a*
622 *Paleoproterozoic volcanic arc complex in the Kedougou Inlier, eastern Senegal.* West Afr. J.
623 Afr. Earth Sci. 24, 197-213.
- 624 Diallo, D.P., 1994. *Caractérisation d'une portion de croûte d'âge protérozoïque inférieur du craton*
625 *Ouest-africain : cas de l'encaissant des granitoïdes dans le super-groupe de Mako (boutonnière*
626 *de Kédougou). Implications géodynamiques.* Thèse de doctorat d'état Univ. Cheikh Anta Diop,
627 Dakar, Sénégal. 466 p.
- 628 Diallo, D.P., 1983. *Contribution à l'étude géologique de la série du Dialé (Birimien) dans les monts*
629 *Bassaris-sénégal oriental (secteur de Bandafassi-Ibel-Ndébou-Landiéné).* Thèse de 3ème cycle
630 Univ. Cheikh Anta Diop, Dakar, Sénégal. 181 p.
- 631 Dioh, E., 1995. *Caractérisation, signification et origine des formations birimiennes encaissantes du*
632 *granite de Dioumbalou (Partie septentrionale de la boutonnière de Kédougou-Sénégal oriental).*
633 Thèse de doctorat d'état Univ. Cheikh Anta Diop, Dakar, Sénégal. 425 p.
- 634 Dioh, E., 1986. *Etude des roches magmatiques Birimiennes de la région de Sonfara- Laminia- Médina*
635 *Foulbé (Sénégal oriental).* Thèse de doctorat 3ème cycle Univ. Nancy I, France. 144 p.
- 636 Dioh, E., Béziat, D., Debat, P., Grégoire, M., Ngom, P.M., 2006. *Diversity of the Palaeoproterozoic*
637 *granitoids of the Kédougou inlier (eastern Sénégal): Petrographical and geochemical*
638 *constraints.* J. Afr. Earth Sci. 44, 351-371.
- 639 Dioh, E., Debat, P., Dia, A., Pons, J., Rocci, G., Rollet, M., 1990. *Caractérisation d'un complexe rubané*
640 *dans les formations Birimiennes de la partie septentrionale de la boutonnière de Kédougou -*
641 *Kéniéba.* C. R. Acad. Sci. Paris, Sér. 2, 310, 935-940.
- 642 Doumbia, S., Pouclet, A., Kouamelan, A., Peucat, J.J., Vidal, M., Delor, C., 1998. *Petrogenesis of*
643 *juvenile-type Birimian (Paleoproterozoic) granitoids in Central Côte-d'Ivoire, West Africa:*
644 *geochemistry and geochronology.* Precambrian Res. 87, 33-63.

- 645 Drouin, M., Godard, M., Ildefonse, B., Bruguier, O., Garrido, C.J., 2009. [Geochemical and petrographic](#)
646 evidence for magmatic impregnation in the oceanic lithosphere at Atlantis Massif, Mid-Atlantic
647 Ridge (IODP Hole U1309D, 30°N). *Chem. Geol.* 264, 71-88.
- 648 Furnes, H., Dilek, Y., de Wit, M., 2015. [Precambrian greenstone sequences represent different ophiolite](#)
649 types. *Gondwana Res.* 27, 649-685.
- 650 Gasquet, D., Barbey, P., Adou, M., Paquette, J., 2003. [Structure, Sr-Nd isotope geochemistry and zircon](#)
651 [U-Pb geochronology of the granitoids of the Dabakala area \(Côte d'Ivoire\): evidence for a 2.3](#)
652 [Ga crustal growth event in the Palaeoproterozoic of West Africa. Precambrian Res.](#) 127, 329-
653 354.
- 654 Gozo, A., 2017. [Pétrologie du volcanisme paléoprotérozoïque calco-alcalin du groupe de Mako \(Sénégal](#)
655 [Oriental\) : incidences géotectoniques. Thèse de doctorat unique Univ. Cheikh Anta Diop,](#)
656 [Dakar, Sénégal. 182 p.](#)
- 657 Gozo, A., Diène, M., Diallo, D.P., Dioh, E., Gueye, M., Ndiaye, P.M., 2015. [Petrological and Structural](#)
658 [Approach to Understanding the Mechanism of Formation and Development of Paleoproterozoic](#)
659 [Calc-Alkaline Volcanic Rocks of West Africa's Craton: An example of the Mako and Foulde](#)
660 [Groups \(Kedougou Inlier in Eastern Senegal\). Int. J. Geosci.](#) 6, 675-691.
- 661 Grant, T.B., Larsen, R.B., Anker-Rasch, L., Grannes, K.R., Iljina, M., McEnroe, S., Nikolaisen, E.,
662 Schanche, M., Øen, E., 2016. [Anatomy of a deep crustal volcanic conduit system; The Reinfjord](#)
663 [Ultramafic Complex, Seiland Igneous Province, Northern Norway. Lithos](#) 252–253, 200-215.
- 664 Griffin, W.L., 2008. [Laser Ablation ICP-MS in the Earth Sciences : Current practices and outstanding](#)
665 [Issues. Mineral. Assoc. Can.](#) 40, 308-311.
- 666 Gruau, G., Griffiths, J.B., Lécuyer, C., 1998. [The origin of U-shaped rare earth patterns in ophiolite](#)
667 [peridotites: assessing the role of secondary alteration and melt/rock reaction. Geochim.](#)
668 [Cosmochim. Acta](#) 62, 3545-3560.
- 669 Gueye, M., Ngom, P.M., Diène, M., Thiam, Y., Siegesmund, S., Wemmer, K., Pawlig, S., 2008.
670 [Intrusive rocks and tectono-metamorphic evolution of the Mako Paleoproterozoic belt \(Eastern](#)
671 [Senegal, West Africa\). J. Afr. Earth Sci.](#) 50, 88-110.
- 672 Gueye, M., Siegesmund, S., Wemmer, K., Pawlig, S., Drobe, M., Notle, N., 2007. [New evidences for](#)
673 [an Early Birimian evolution in the West African Craton: An example from the Kedougou](#)
674 [Kenieba inlier, SE- Senegal. South Afr. J. Geol.](#) 110, 179-190.
- 675 Hawkesworth, C., Cawood, P., Dhuime, B., 2013. [Continental growth and the crustal record.](#)
676 [Tectonophysics](#) 609, 651-660.
- 677 Jacobsen, S.B., Quick, J.E., Wasserburg, G.J., 1984. [A Nd and Sr isotopic study of the Trinity peridotite;](#)
678 [implications for mantle evolution. Earth Planet. Sci. Lett.](#) 68, 361-378.
- 679 Jagoutz, O., Muntener, O., Burg, J., Ulmer, P., Jagoutz, E., 2006. [Lower continental crust formation](#)
680 [through focused flow in km-scale melt conduits: The zoned ultramafic bodies of the Chilas](#)
681 [Complex in the Kohistan island arc \(NW Pakistan\). Earth Planet. Sci. Lett.](#) 242, 320-342.

- 682 Koga, K.T., Kelemen, P.B., Shimizu, N., 2001. Petrogenesis of the crust-mantle transition zone and the
683 origin of lower crustal wehrlite in the Oman ophiolite: petrogenesis of the crust-mantle
684 transition zone. *Geochem. Geophys. Geosyst.* 2, N° 9.
- 685 Lambert-Smith, J.S., Lawrence, D.M., Müller, W., Treloar, P.J., 2016. Palaeotectonic setting of the
686 south-eastern Kédougou-Kéniéba Inlier, West Africa: New insights from igneous trace element
687 geochemistry and U-Pb zircon ages. *Precambrian Res.* 274, 110-135.
- 688 Lanphere, M.A., Irwin, W.P., Hotz, P.E., 1968. Isotopic age of the Nevadan orogeny and older plutonic
689 and metamorphic events in the Klamath Mountains, California. *Geol. Soc. Am. Bull.* 79, 1027-
690 1052.
- 691 Lawrence, D.M., 2010. Characterisation and evolution of Au mineralization in the Loulo mining district,
692 Western Mali. Unpublished Ph.D. thesis, London, Kingston Univ. 341 p.
- 693 Lawrence, D.M., Treloar, P.J., Rankin, A.H., Harbridge, P., Holliday, J., 2013. The Geology and
694 Mineralogy of the Loulo Mining District, Mali, West Africa: Evidence for Two Distinct Styles
695 of Orogenic Gold Mineralization. *Econ. Geol.* 108, 199-227.
- 696 Leake, B.E., Woolley, A.R., Birch, W.D., Burke, E.A.J., Ferraris, G., Grice, J.D., Hawthorne, F.C.,
697 Kisch, H.J., Krivovichev, V.G., Schumacher, J.C., Stephenson, N.C.N., Whittaker, E.J.W.,
698 2003. Nomenclature of amphiboles: additions and revisions to the International Mineralogical
699 Association's amphibole nomenclature. *Can Miner.* 41, 1355-1370.
- 700 Ledru, P., Pons, J., Milesi, J., Feybesse, J., Johan, V., 1991. Transcurrent tectonics and polycyclic
701 evolution in the Lower Proterozoic of Senegal-Mali. *Precambrian Res.* 50, 337-354.
- 702 Loh, G., Hirdes, W., 1999. Explanatory Notes for the Geological Map of Southwest Ghana 1:100,000
703 Sekondi (0402A) and Axim (0403B) Sheets. *Geol. Surv. Bull.* 49, 149.
- 704 Masurel, Q., Thébaud, N., Miller, J., Ulrich, S., Hein, K.A.A., Cameron, G., Béziat, D., Bruguier, O.,
705 Davis, J.A., 2017. Sadiola Hill: A World-Class Carbonate-Hosted Gold Deposit in Mali, West
706 Africa. *Econ. Geol.* 112, 23-47.
- 707 Milesi, J., Feybesse, J., Pinna, P., Deschamps, Y., Kampunzu, H., Muhongo, S., Lescuyer, J.L., Le
708 Goff, E., Delor, C., Billa, M., Ralay, F., Heinry, C., 2004. Geological map of Africa 1:10000000
709 SIGAfrique project. In: 20th Conference of African Geology, BRGM, Orleans, France, 2-7
710 June, <http://www.sigafrique.net> (lastaccessed 14/12/2010).
- 711 Morimoto, N., Fabriés, J., Ferguson, A.K., Ginsburg, L.V., Ross, M., Seifert, F.A., Zussman, J., AoKi,
712 K., Gottardi, G., 1988. Nomenclature of pyroxenes (subcommitee on pyroxene, IMA.). *Mineral.*
713 *Mag.* 52, 535-550.
- 714 Myers, J.S., Shaw, R.D., Tyler, I.M., 1996. Tectonic evolution of Proterozoic Australia. *Tectonics* 15,
715 1431-1446.
- 716 Ngom, P.M., 1995. Caractérisation de la croûte Birimienne dans les parties centrale et méridionale du
717 supergroupe de Mako. Implications géochimiques et pétrogénétiques. Thèse de doctorat d'état
718 Univ. Cheikh Anta Diop, Dakar, Sénégal. 240 p.

- 719 Ngom, P.M., 1989. Caractères géochimiques des formations Birimiennes du supergroupe de Mako
720 (Sabodala et ses environs). Afr. Earth Sci. 8, 91-97.
- 721 Ngom, P.M., 1985. Contribution à l'étude de la série Birimienne de Mako dans le secteur de Sabodala
722 (Sénégal oriental). Thèse de 3ème cycle Univ. Nancy I, France. 134 p.
- 723 Ngom, P.M., Cissokho, S., Gueye, M., Joron, J.-L., 2011. Diversité du volcanisme et évolution
724 géodynamique au Paléoprotérozoïque : exemple du Birimien de la boutonnière de Kédougou-
725 Kéniéba (Sénégal). Afr. Geosci. Rev. 18, 1-22.
- 726 Ngom, P.M., Cordani, U.G., Teixeira, W., Janasi, V. de A., 2010. Sr and Nd isotopic geochemistry of
727 the early ultramafic–mafic rocks of the Mako bimodal volcanic belt of the Kedougou–Kenieba
728 inlier (Senegal). Arab. J. Geosci. 3, 49-57.
- 729 Ngom, P.M., Gueye, M., Cissokho, S., Joron, J.-L., Treuil, M., Dabo, M., 2007. Signification
730 géodynamique des roches volcaniques dans les ceintures de roches vertes d'âge
731 paléoprotérozoïque; Exemple de la partie méridionale du supergroupe de Mako, boutonnière de
732 Kédougou (Sénégal). Approche des éléments en traces. J. Sci. Technol. 5, 52-71.
- 733 Ngom, P.M., Rocci, G., Debat, P., Dia, A., Diallo, D.P., Dioh, E., Sylla, M., 1998. Les massifs basiques
734 et ultrabasiques Birimiens du supergroupe de Mako (Sénégal oriental): Pétrographie, géochimie
735 et signification pétrogénétique. Bull. L'IFAN Cheikh Anta Diop, Dakar, Sénégal, T.49, Sér. A,
736 N° 2, pp. 33-54.
- 737 Nicolle, M., Jousselin, D., Reisberg, L., Bosch, D., Stephan, A., 2016. Major and trace element and Sr
738 and Nd isotopic results from mantle diapirs in the Oman ophiolite: Implications for off-axis
739 magmatic processes. Earth Planet. Sci. Lett. 437, 138-149.
- 740 Olierook, H.K.H., Sheppard, S., Johnson, S.P., Occhipinti, S.A., Reddy, S.M., Clark, C., Fletcher, I.R.,
741 Rasmussen, B., Zi, J.-W., Pirajno, F., LaFlamme, C., Do, T., Ware, B., Blandthorn, E., Lindsay,
742 M., Lu, Y.-J., Crossley, R.J., Erickson, T.M., 2018. Extensional episodes in the
743 Paleoproterozoic Capricorn Orogen, Western Australia, revealed by petrogenesis and
744 geochronology of mafic–ultramafic rocks. Precambrian Res. 306, 22-40.
- 745 Ouédraogo, A., 1985. Etude de quelques unités plutoniques basiques éburnéennes dans le sillon de
746 Bouroum Yalogo au NE du Burkina Faso. Thèse de doctorat 3ème cycle Univ. Nancy I, France.
747 64 p.
- 748 Parra Avila, L.A., Kemp, A.I.S., Fiorentini, M.L., Belousova, E., Baratoux, L., Block, S., Jessell, M.,
749 Davis, J., McCuaig, T.C., 2017. The geochronological evolution of the Paleoproterozoic
750 Baoulé-Mossi domain of the southern West African Craton. Precambrian Res. 300, 1-27.
- 751 Pawlig, S., Gueye, M., Klischies, R., Schwarz, S., 2006. Geochemical and Sr – Nd isotopic data on
752 Birimian formations of the Kedougou – Kéniéba Inlier (Eastern Senegal): Implications of the
753 Paleoproterozoic evolution of the West African Craton. South Afr. J. Geol. 109, 407-423.
- 754 Pearce, J.A., Cann, J.R., 1973. Tectonic setting of basic volcanic rocks determined using trace element
755 analyses. Earth Planet. Sci. Lett. 19, 290-300.

- 756 Pin, C., Briot, D., Poitrasson, F., 1994. Concomitant separation of strontium and samarium-neodymium
757 for isotopic analysis in silicate samples, based on specific extraction chromatography. *Anal.*
758 *Chim. Acta* 298, 209-217.
- 759 Pirajno, F., 2004. Oceanic plateau accretion onto the northwestern margin of the Yilgarn Craton,
760 Western Australia. *J. Geodyn.* 37, 205-231.
- 761 Pirajno, F., Occhipinti, S.A., 2000. Three Palaeoproterozoic basins-Yerrida, Bryah and Padbury-
762 Capricorn Orogen, Western Australia. *Aust. J. Earth Sci.* 47, 675-688.
- 763 Pouclet, A., Doumbia, S., Vidal, M., 2006. Geodynamic setting of Birimian volcanism in central Ivory
764 Coast (western Africa) and its place in the Paleoproterozoic evolution of the Man Shield. *Bull.*
765 *Soc. Géol. Fr. t.* 177, 105-121.
- 766 Python, M., Ceuleneer, G., 2003. Nature and distribution of dykes and related melt migration structures
767 in the mantle section of the Oman ophiolite: Oman ophiolite dykes. *Geochem. Geophys.*
768 *Geosyst.* 4.
- 769 Roddaz, M., Debat, P., Nikiéma, S., 2007. Geochemistry of Upper Birimian sediments (major and trace
770 elements and Nd-Sr isotopes) and implications for weathering and tectonic setting of the Late
771 Paleoproterozoic crust. *Precambrian Res.* 159, 197-211.
- 772 Rospabé, M., Benoit, M., Ceuleneer, G., Hodel, F., Kaczmarek, M.-A., 2018. Extreme geochemical
773 variability through the dunitic transition zone of the Oman ophiolite: Implications for melt/fluid-
774 rock reactions at Moho level beneath oceanic spreading centers. *Geochim. Cosmochim. Acta*
775 234, 1–23.
- 776 Sangaré, A., 2008. Les roches ultramafiques et mafiques Paléoprotérozoïques de la ceinture de roches
777 vertes de Kadiolo (Mali). Pétrologie, évolution et ressources minérales associées. Mémoire de
778 fin d'études. Master géosciences et ressources minérales, département des Sciences de la Terre,
779 Univ. Sidi Mohamed Ben Abdellah, Maroc. 67 p.
- 780 Sun, S.-S., McDonough, W.F., 1989. Chemical and isotopic systematics of oceanic basalts: implications
781 for mantle composition and processes. *Geol. Soc. Lond. Spec. Publ.* 42, 313-345.
- 782 Sylvester, P.J., Attoh, K., 1992. Lithostratigraphy and composition of 2.1 Ga greenstone belts of the
783 West African Craton and their bearing on crustal evolution and Archean-Proterozoic boundary.
784 *J. Geol.* 100, 377-393.
- 785 Theveniaut, H., Ndiaye, P., Buscail, F., Coueffe, R., Delor, C., Fullgraf, T., Goujou, J.C., 2010. Notice
786 explicative de la carte géologique du Sénégal oriental à 1/500000. Ministère des Mines, de
787 l'industrie de l'agro-industrie et des PME, Direction des mines et de la géologie, Dakar. 120
788 p.
- 789 Winchester, J.A., Floyd, P.A., 1976. Geochemical magma type discrimination : application to altered and
790 metamorphosed basic igneous rocks. *Earth Planet. Sci. Lett.* 28 (3), pp. 459-469.

791 Wood, D.A., Joron, J.-L., Treuil, M., 1979. A re-appraisal of the use of trace elements to classify and
792 discriminate between magma series erupted in different tectonic settings. *Earth Planet. Sci. Lett.*
793 45, 326-336.
794 Yokoyama, T., Makishima, A., Nakamura, E., 1999. Evaluation of the coprecipitation of incompatible
795 trace elements with fluoride during silicate rock dissolution by acid digestion. *Chem. Geol.* 157,
796 175-187.
797 Yu, X., Lee, C.T.A., Chen, L.H., Zeng, G., 2015. Magmatic recharge in continental flood basalts:
798 insights from the Chifeng Igneous Province in inner Mongolia. *Geochem. Geophys. Geosyst.*
799 16, 2082-2096.
800 Yuan, L., Zhang, X., Yang, Z., Lu, Y., Chen, H., 2017. Paleoproterozoic Alaskan-type ultramafic-mafic
801 intrusions in the Zhongtiao mountain region, North China Craton: Petrogenesis and tectonic
802 implications. *Precambrian Res.* 296, 39-61.
803

804 **Fig. 1:** Geological map of the West African craton (Milési et al., 2004 modified). Zone 1,
805 Katiola-Marabadiassa belt (Ivory coast; Pouclet et al., 2006); zone 2, Dixcove and Ashanti belts
806 (Ghana; Attoh et al., 2006 and Dampare et al., 2019 respectively); zone 3, Boromo belt (Burkina
807 Faso; Ouédraogo, 1985; Béziat et al., 2000; Castaing et al., 2003); zone 4, Kadiolo belt (Mali;
808 Sangaré, 2008) and zone 5, Mako region (Eastern Senegal; Bassot, 1966; Dia, 1988; Ngom,
809 1995; Ngom et al., 1998 and 2010; Cissokho, 2010; Dabo et al., 2017).

810 **Fig. 2:** Geological map of the Kedougou - Kenieba Inlier (modified from Dioh et al., 2006).

811 **Fig. 3:** (a) Interpretative geological map of the Mako area (modified from Théveniaut et al.,
812 2010); b) and c) close-up views of UB outcrops from Mako – Lame and Koulountou sectors
813 respectively with the localization of sampling sites (yellow dots). The numbers 1 to 7
814 represent the different UB massifs.

815 **Fig. 4:** Photomicrographs: (a and b) granular (*IL9, IL10*) and (c) porphyritic lherzolites (*IL12*)
816 showing poikilitic orthopyroxene phenocrysts including small crystals of olivine and
817 clinopyroxene; (d) harzburgite (*IL51*) showing olivine crystals encompassed by the poikilitic
818 orthopyroxene and amphibole crystals; (e) wehrlite (*IL32*) showing intercumulus clinopyroxene
819 and cumulus olivine completely altered in serpentine and Fe-oxides and (f) wehrlite (*ILL3*)
820 showing poikilitic crystals of clinopyroxene and orthopyroxene including crystals of olivine
821 partially or totally altered. Ol = olivine; Cpx = clinopyroxene; Opx = orthopyroxene; SOl =
822 Serpentinized Olivine.

823 **Fig. 5:** Compositional variation of (a) pyroxene ([Morimoto et al., 1988](#)); (b) primary
824 amphibole ([Leake, 2003](#)) and (c) oxides from the UB rocks in the Mako sector.

825 **Fig. 6:** Harker diagrams of Mako UB rocks compared to other UB rocks from the WAC. The
826 data on Mako are from [Ngom et al., 2010](#), those of Loraboué ([Béziat et al., 2000](#)), Bouroum
827 Yalogo, NE Burkina Faso ([Ouédraogo, 1985](#)), Katiola-Marabadiassa, Central Ivory Coast
828 ([Pouclet et al., 2006](#)), Kadiolo, Mali ([Sangaré, 2008](#)), Dixcove greenstone belt ([Attoh et al.,
829 2006](#)) and Southern Ashanti volcanic belt ([Dampare et al., 2019](#)), Ghana.

830 **Fig. 7:** (a, c, e, g, i) Chondrite-normalized REE and (b, d, f, h, j) Primitive Mantle-normalized
831 multi-elements patterns of whole rock (WR), clinopyroxene (Cpx) and amphibole (amp) for the
832 Mako and Loraboué UB rocks. Normalizing chondrite and Primitive Mantle values are from
833 [Barrat et al., 2014](#) and [Sun and McDonough, 1989](#) respectively. W : West ; SE : South East.

834 **Fig. 8:** A $\text{Sm}_{\text{PM}}/\text{Yb}_{\text{PM}}$ vs $\text{Nb}_{\text{PM}}/\text{La}_{\text{PM}}$ diagram showing the trace element compositions of whole
835 rock (WR), clinopyroxene (Cpx) and amphibole (amp) for the Mako and Loraboué UB rocks
836 (Normalized to Primitive Mantle using values of [Sun and McDonough, 1989](#)). SE : South East.

837 **Fig. 9 :** (a) Rb/Sr isochron diagram for Mako UB rocks in which an hypothetical 2.1 Ga
838 calculated isochron is reported; (b) Sm/Nd isochron diagram with same assumptions as in (a);
839 (c) ε_{Nd} (2.1 Ga) versus $^{87}\text{Sr}/^{86}\text{Sr}$ (2.1 Ga) diagram in which our samples are compared to all
840 Birimian available data ([Abouchami et al., 1990](#); [Alric, 1990](#); [Boher et al., 1992](#); [Ama Salah et
841 al., 1996](#); [Dia et al., 1997](#); [Gasquet et al., 2003](#); [Pawlig et al., 2006](#); [Dampare et al., 2009](#); [Ngom
842 et al., 2010](#); [Dampare et al., 2019](#)). DM= contemporaneous depleted mantle from Ben Othman
843 et al. (1984).

844 **Fig. 10:** Harker diagrams: composition of chromite (a and b); clinopyroxene (c and d) and
845 primary amphibole (e, f, g, h) of Mako wehrlites compared to the composition of Loraboué
846 wehrlites.

847 **Fig. 11:** A $\text{Tb}_{\text{N}}/\text{Yb}_{\text{N}}$ vs $\text{La}_{\text{N}}/\text{Sm}_{\text{N}}$ diagram showing the trace element compositions of the whole
848 rock and clinopyroxene (Cpx) for the Mako UB rocks compared of the Loraboué wehrlites
849 (Normalized to chondrites using NWA974 values of [Barrat et al., 2014](#)). Full symbols are used
850 for whole rock analyses and open symbols for minerals.

851 **Fig. 12:** A $\text{Gd}_{\text{N}}/\text{Yb}_{\text{N}}$ vs $\text{La}_{\text{N}}/\text{Sm}_{\text{N}}$ diagram showing the trace element compositions for the Mako
852 UB rocks compared with other UB rocks from the WAC ([Béziat et al., 2000](#); [Attoh et al., 2006](#);

853 Pouclet et al., 2006; Sangaré, 2008; Dampare et al., 2009; Ngom et al., 2010; Dampare et al.,
854 2019). Normalized to chondrites using NWA974 values of Barrat et al., 2014.

855 **Fig. 13:** A ϵ_{Nd} (2.1 Ga) versus $\alpha(\text{Sm}/\text{Nd})$ diagram showing the variations of composition for
856 the Mako UB rocks compared with all available data from Birimian magmatic rocks of the
857 WAC (Abouchami et al., 1990; Alric, 1990; Boher et al., 1992; Ama Salah et al., 1996; Dia et
858 al., 1997; Gasquet et al., 2003; Pawlig et al., 2006; Dampare et al., 2009; Ngom et al., 2010;
859 Dampare et al., 2019). Pacific MORB (Cohen et al., 1980; Hofmann et al., 1983; Byers et al.,
860 1986; Macdougall et al., 1986; Hekinian et al., 1989; Natland, 1989; Prinzhofer et al., 1989;
861 Ben othman et al., 1990; Mahoney et al., 1993; Bach et al., 1995; Batiza et al., 1996; Nui et al.,
862 1999; Regelous et al., 1999; Castillo et al., 2000). Marianna arc (Meijer, 1976; Meijer et al.,
863 1981; Hickey et al., 1982; Stern et al., 1984; White et al., 1984; Hawkins et al., 1985; Bloomer
864 et al., 1987; Volpe et al., 1987; Woodhead, 1988; Bloomer et al., 1989; Lin et al., 1989;
865 Hawkins et al., 1990; Stern et al., 1990; Volpe et al., 1990; Hickey-vargas, 1991; Stern et al.,
866 1991; Alt et al., 1993; Stolper et al., 1994; Gribble et al., 1996; Elliott et al., 1997; Pickett et
867 al., 1997; Gribble et al., 1998; Hickey-vargas, 1998; Ikeda et al., 1998; Newman et al., 1999).
868 New Hebrides arc (Peate et al., 1997).

869

870 Table 1 : Representative microprobe analyses of olivines (Lhz : Lherzolite ; Hzb :
871 Harzburgite ; Whr : Wehrlite ; Fo : Forsterite ; Fa : Fayalite)

872 Table 2 : Representative microprobe analyses of clinopyroxenes

873 Table 3: Representative microprobe analyses of orthopyroxenes (En : Enstatite ; Wo :
874 Wollastonite ; Fs : Ferrosilite)

875 Table 4: Representative microprobe analyses of amphiboles

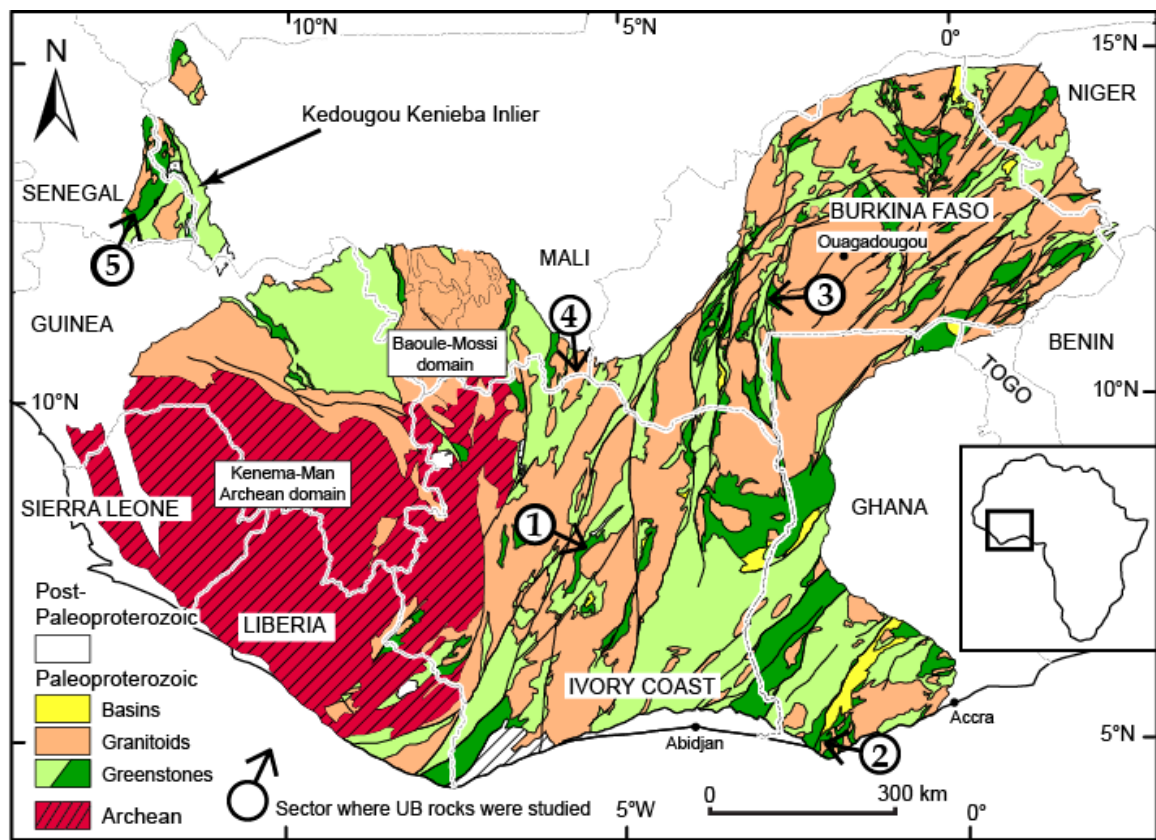
876 Table 5 : Representative microprobe analyses of oxides

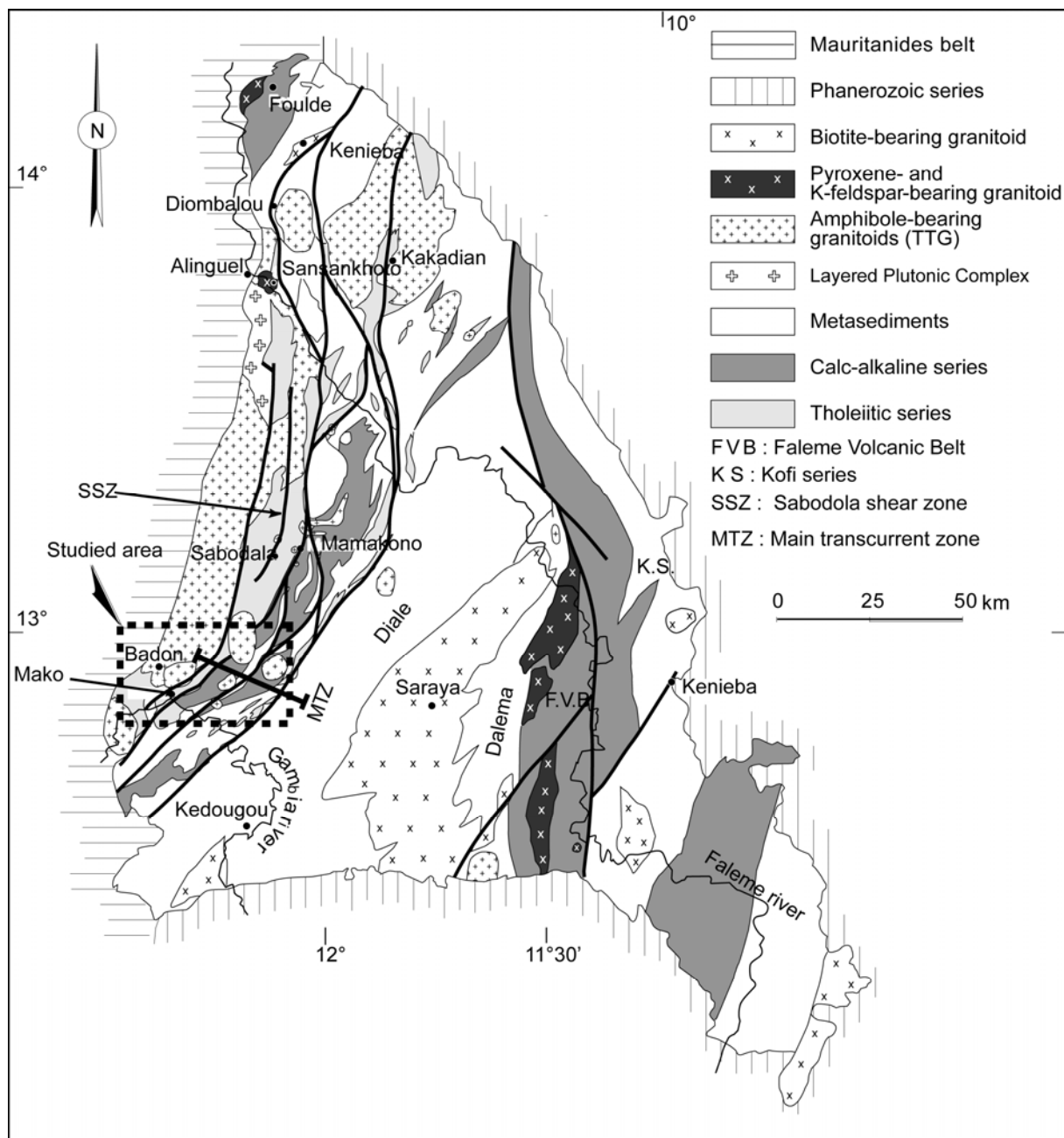
877 Table 6: Whole rock major and trace element concentrations

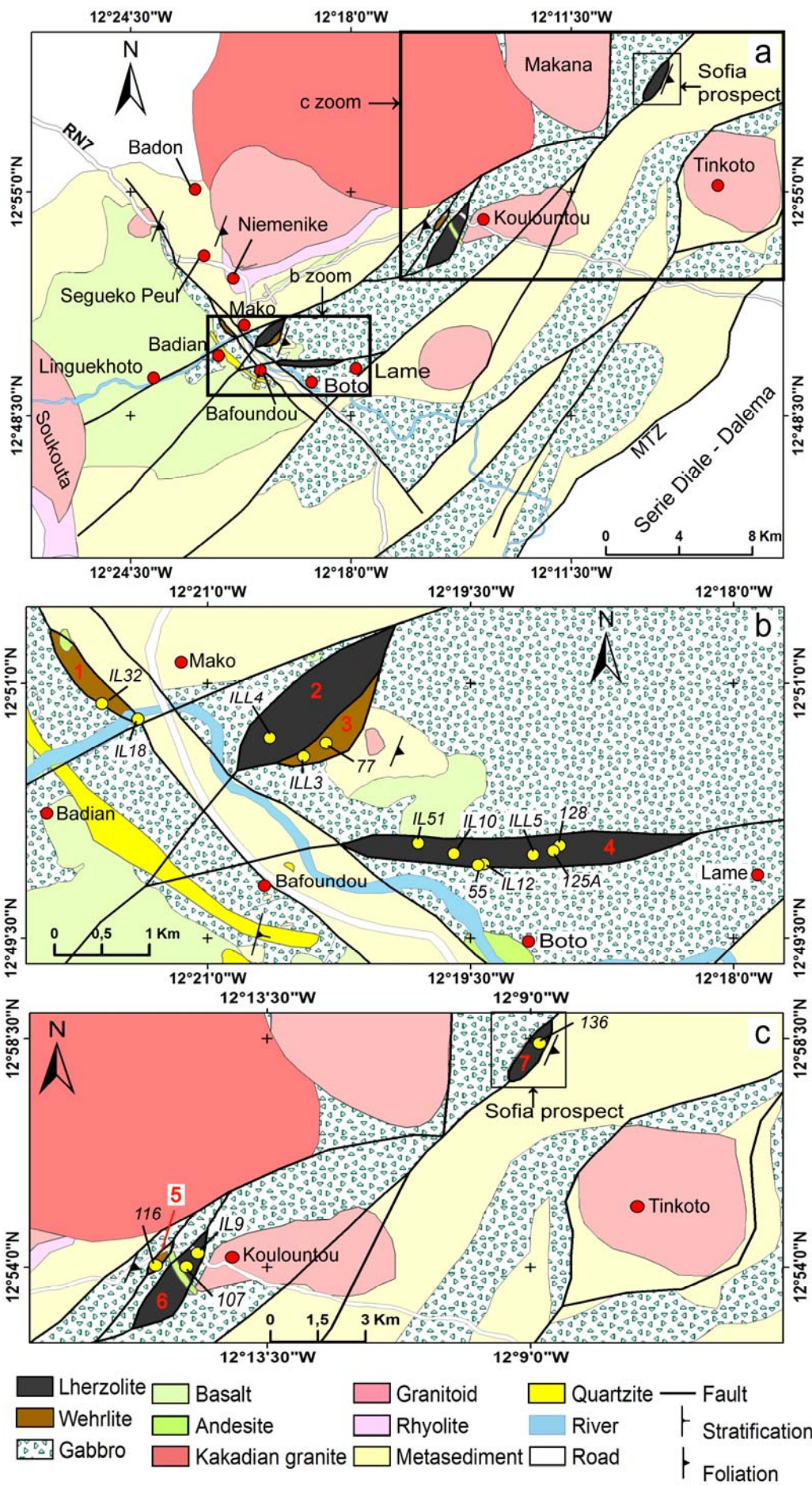
878 Table 7: Trace element analyses of clinopyroxene

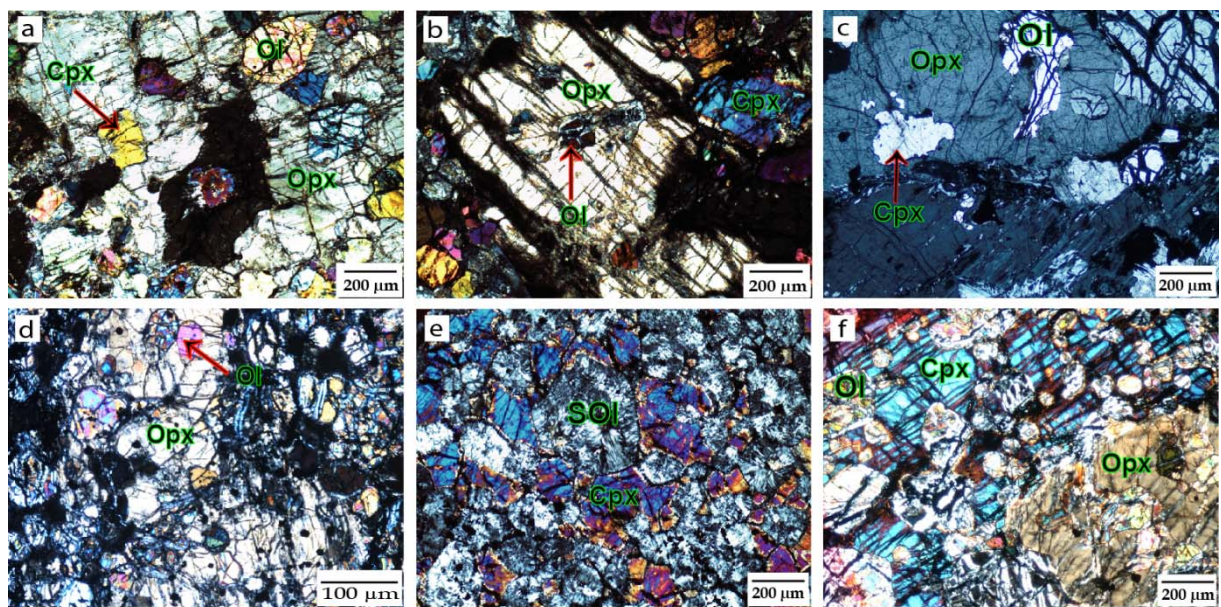
879 Table 8: Trace element analyses of amphibole and clinopyroxene (Cpx : clinopyroxene ;
880 amph : amphibole ; Lhz : Lherzolite ; Whr : wehrelite)

881 Table 9: Summary of the Rb/Sr and Nd/Sm isotopic data

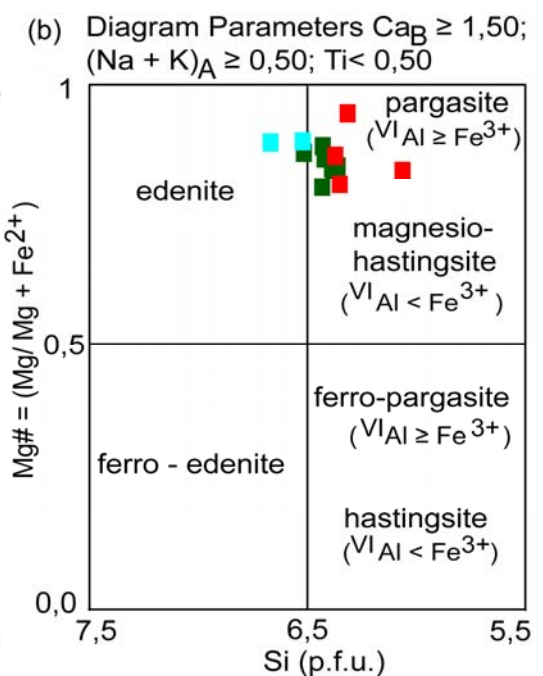
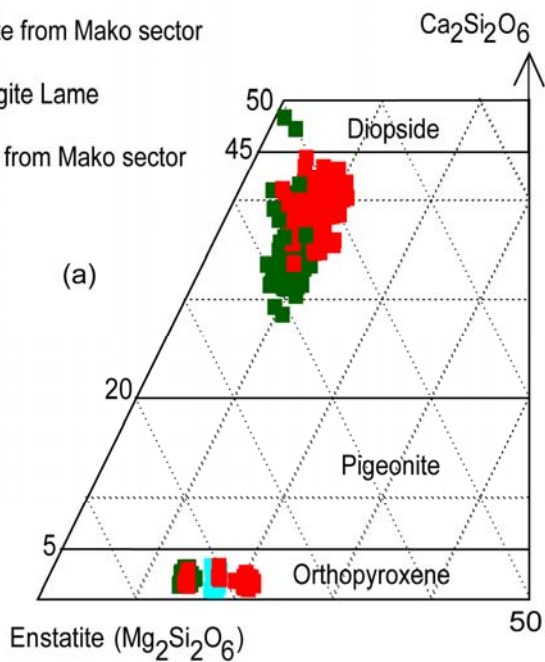


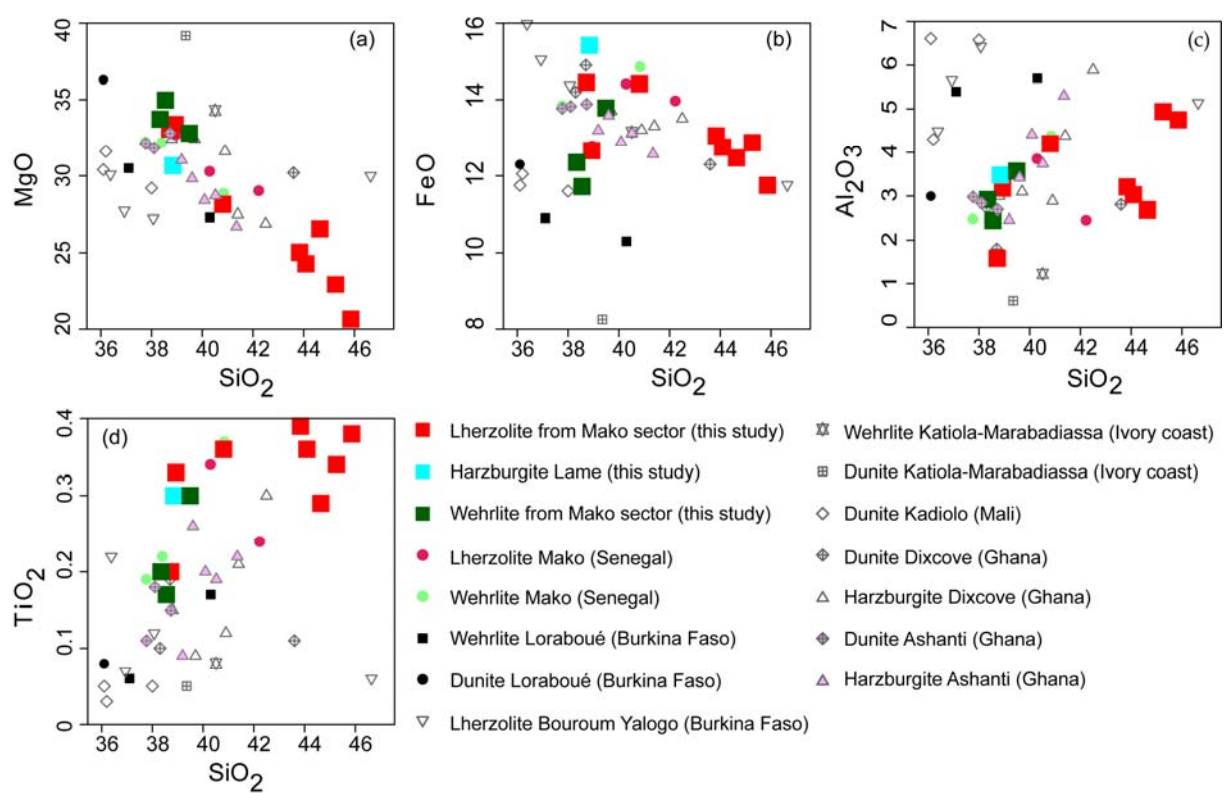
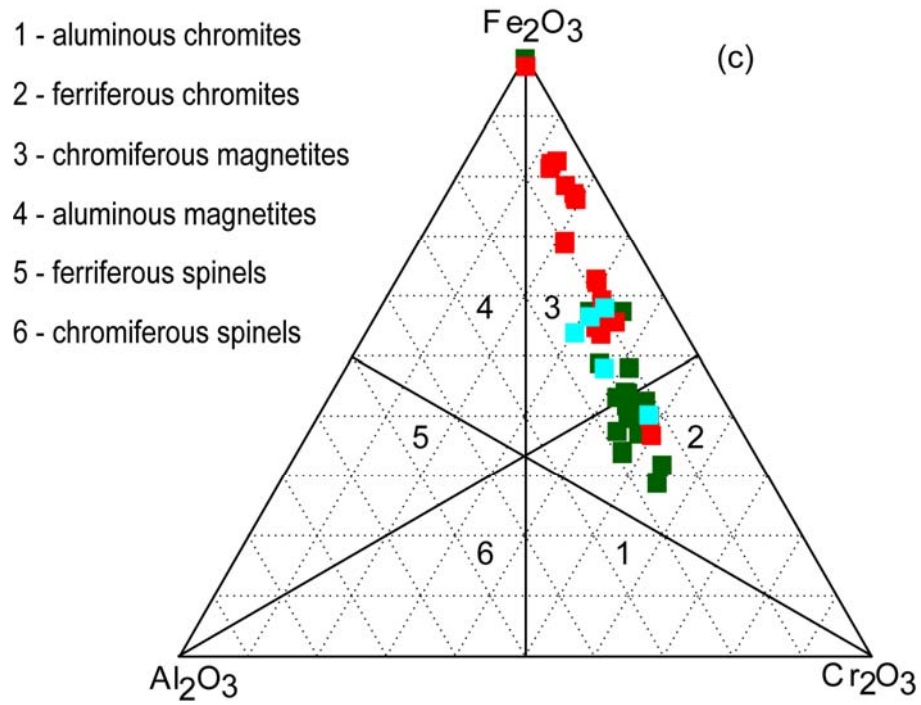


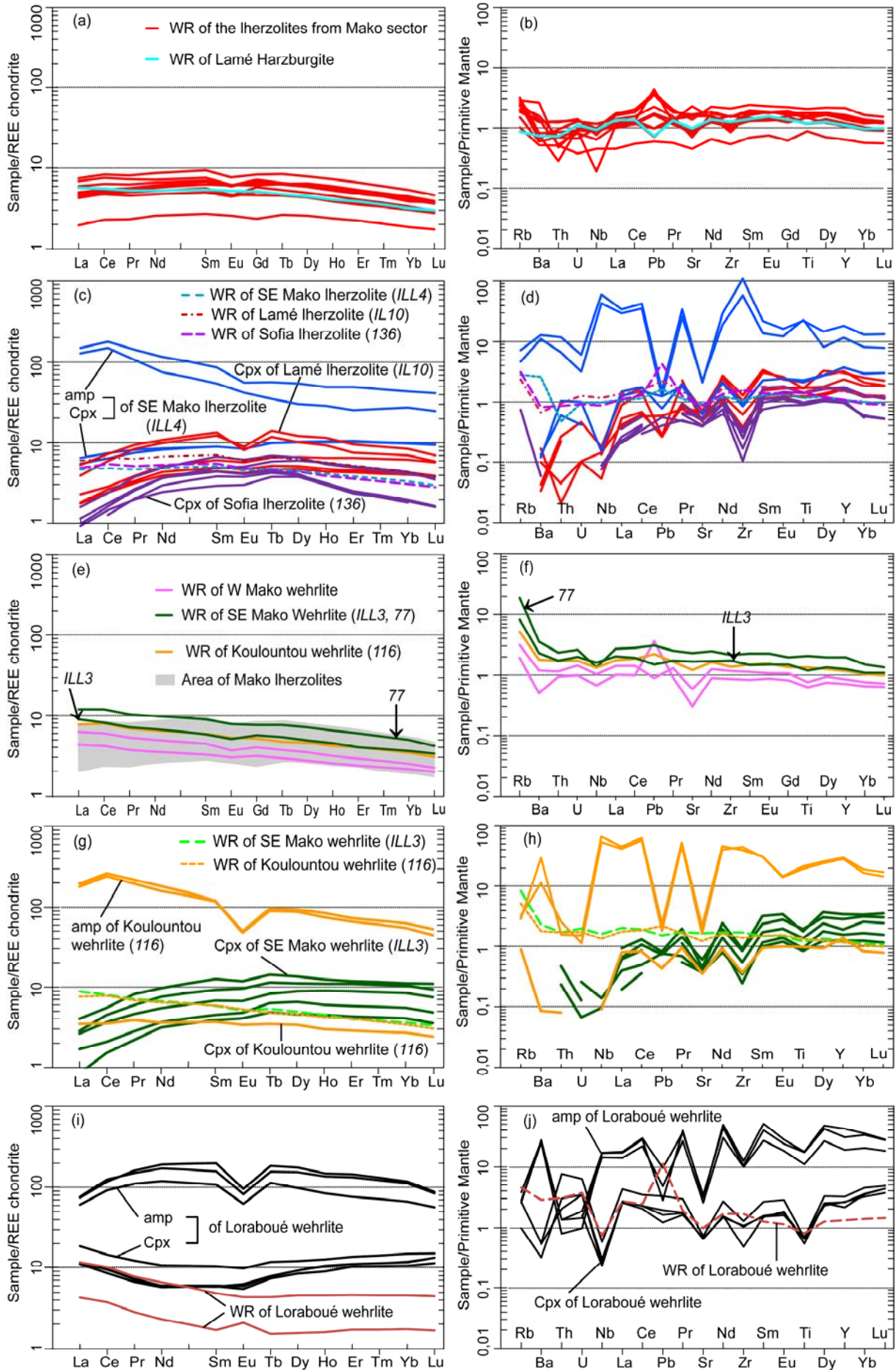


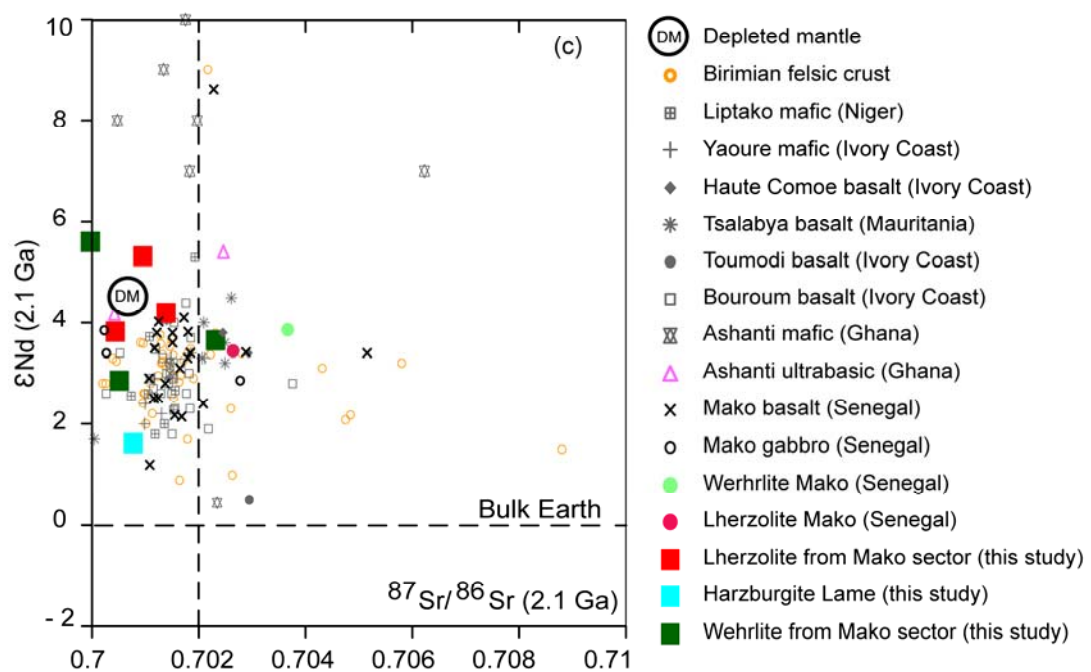
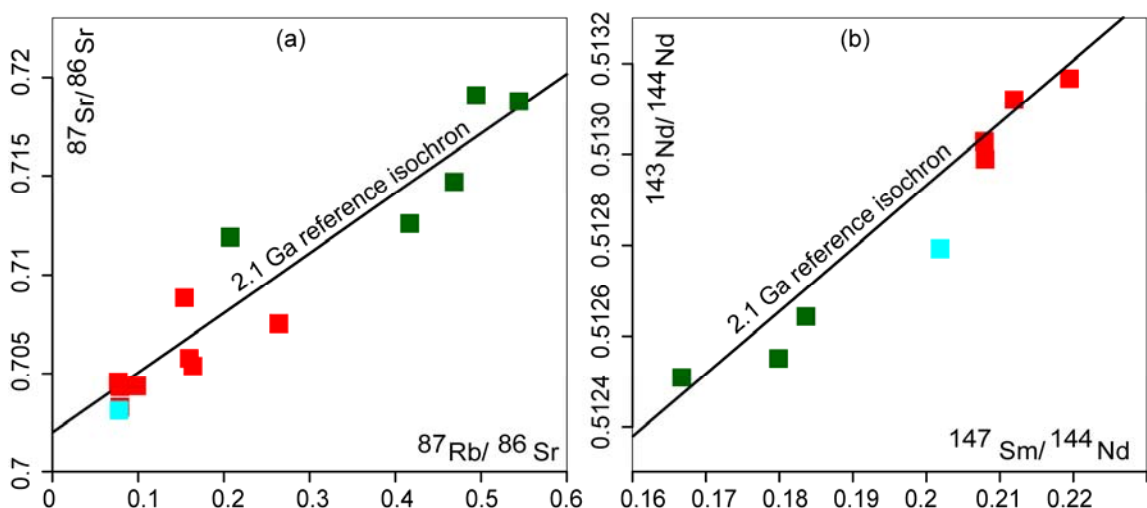
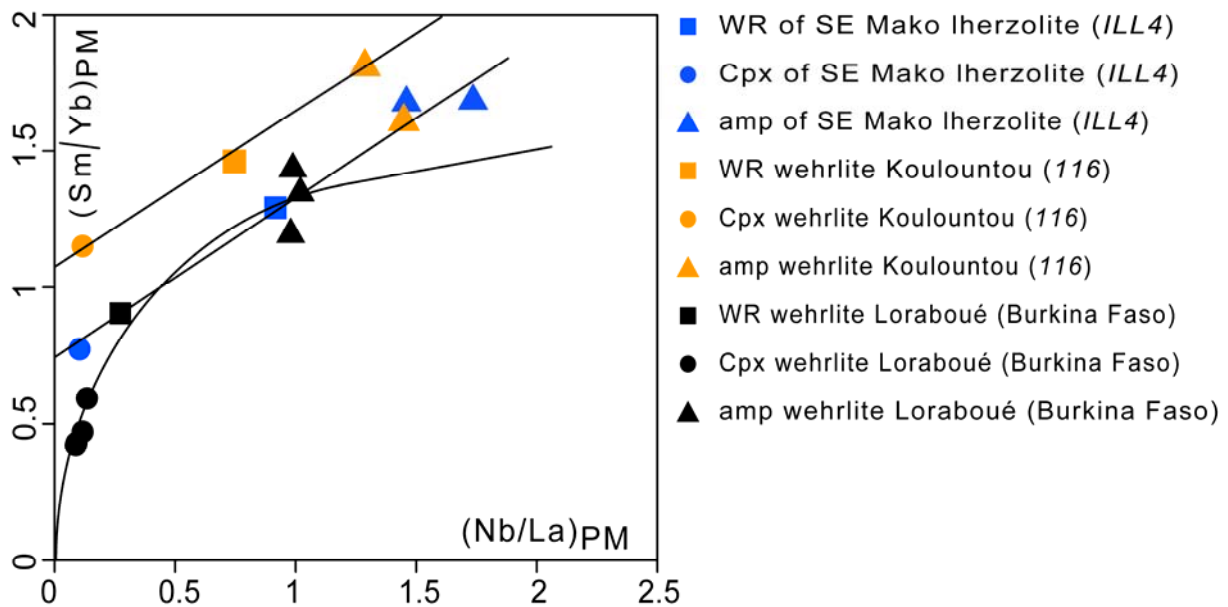


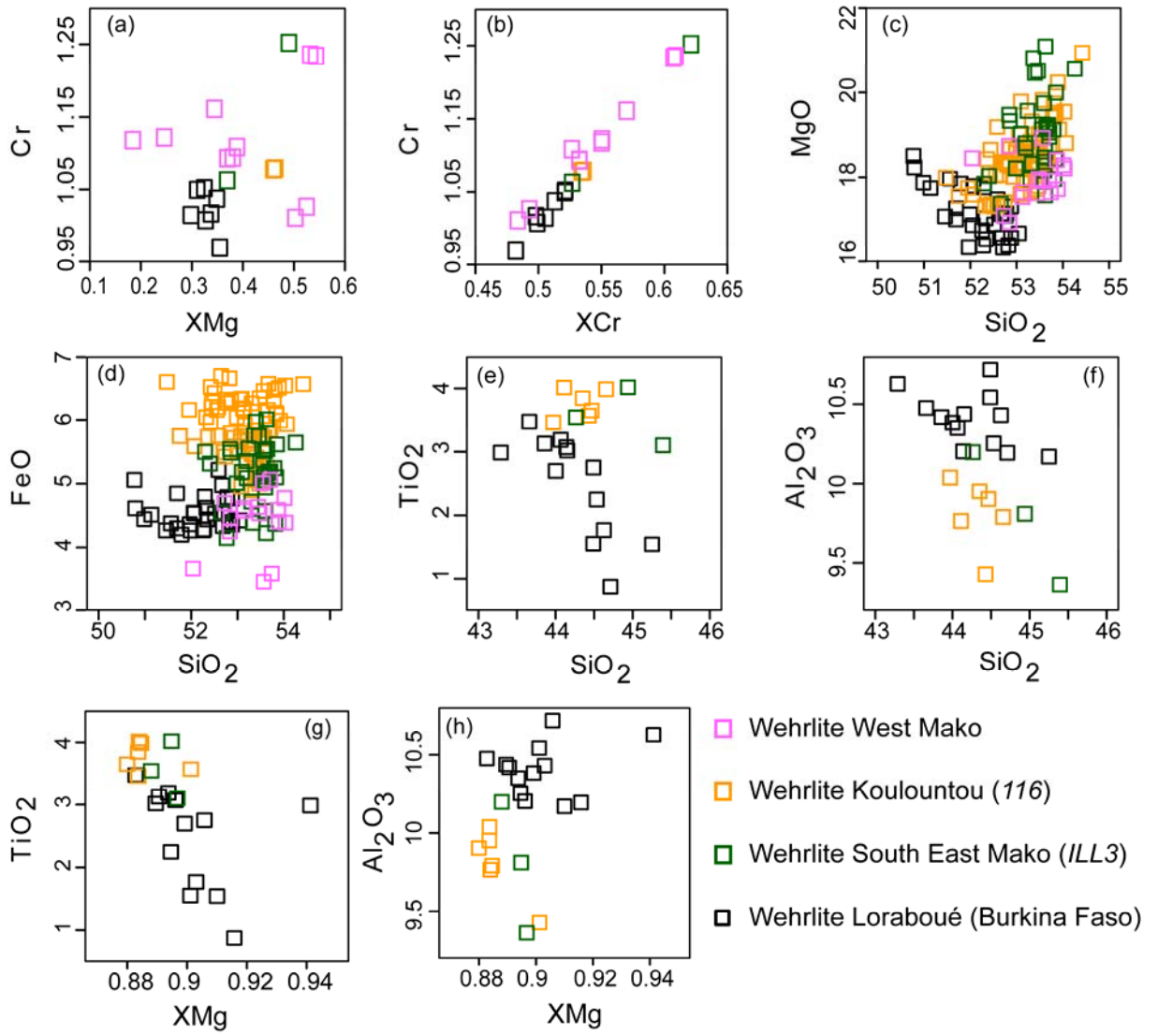
- Lherzolite from Mako sector
- Harzburgite Lame
- Wehrlite from Mako sector

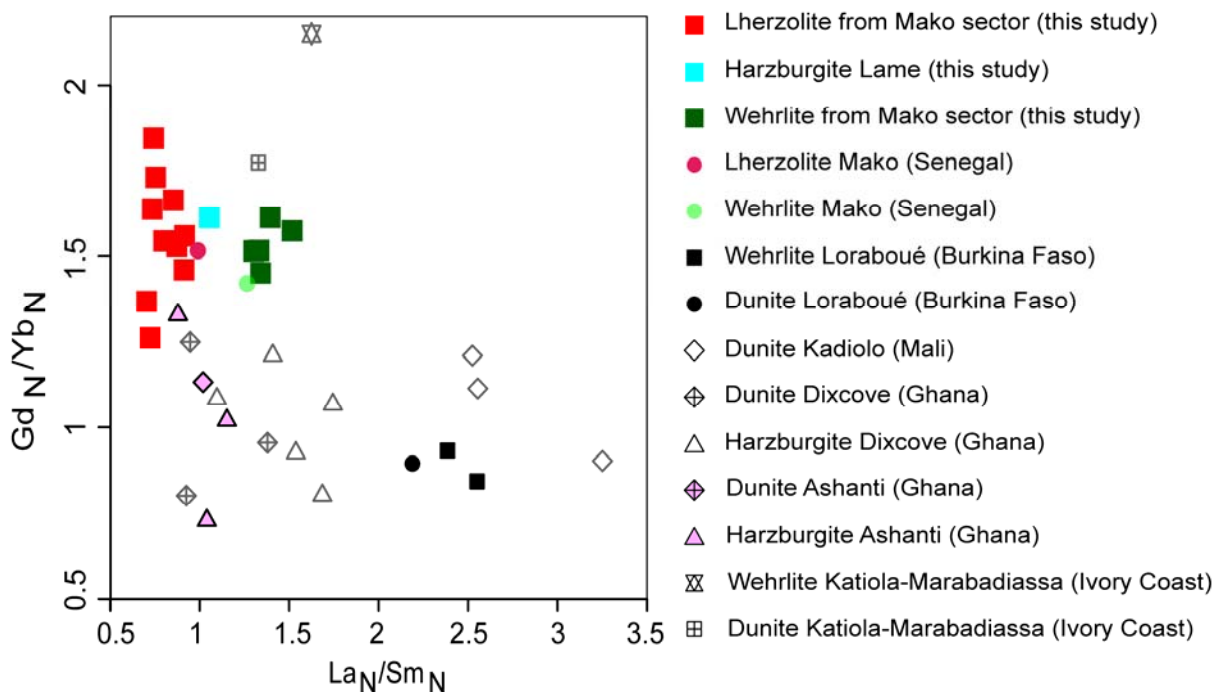
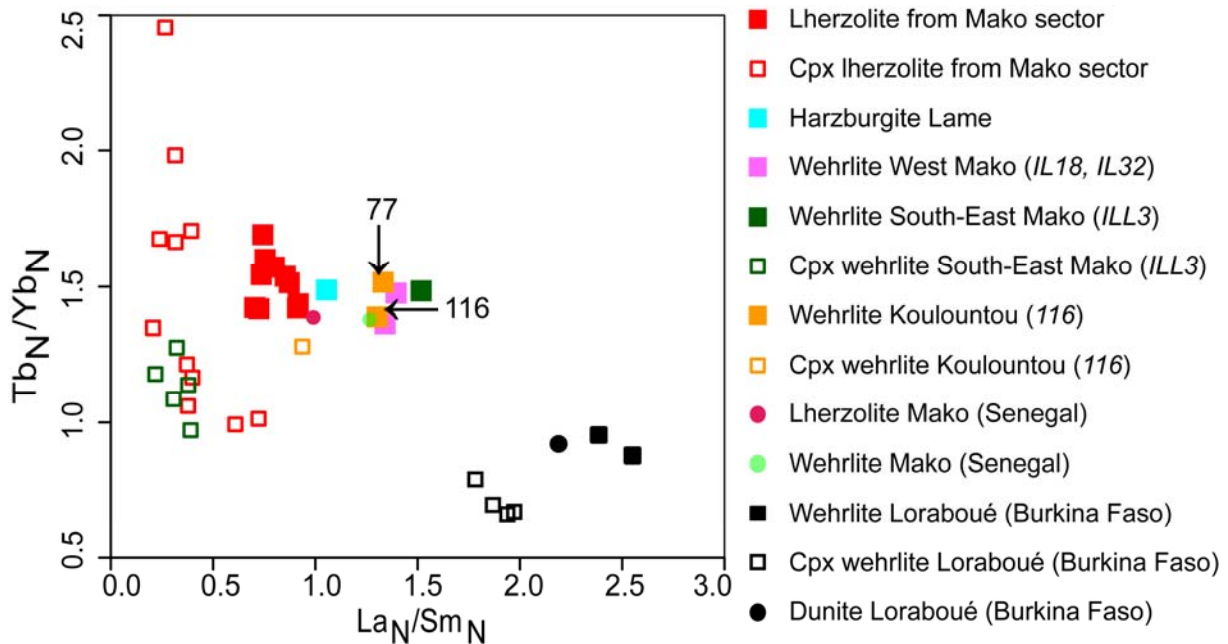












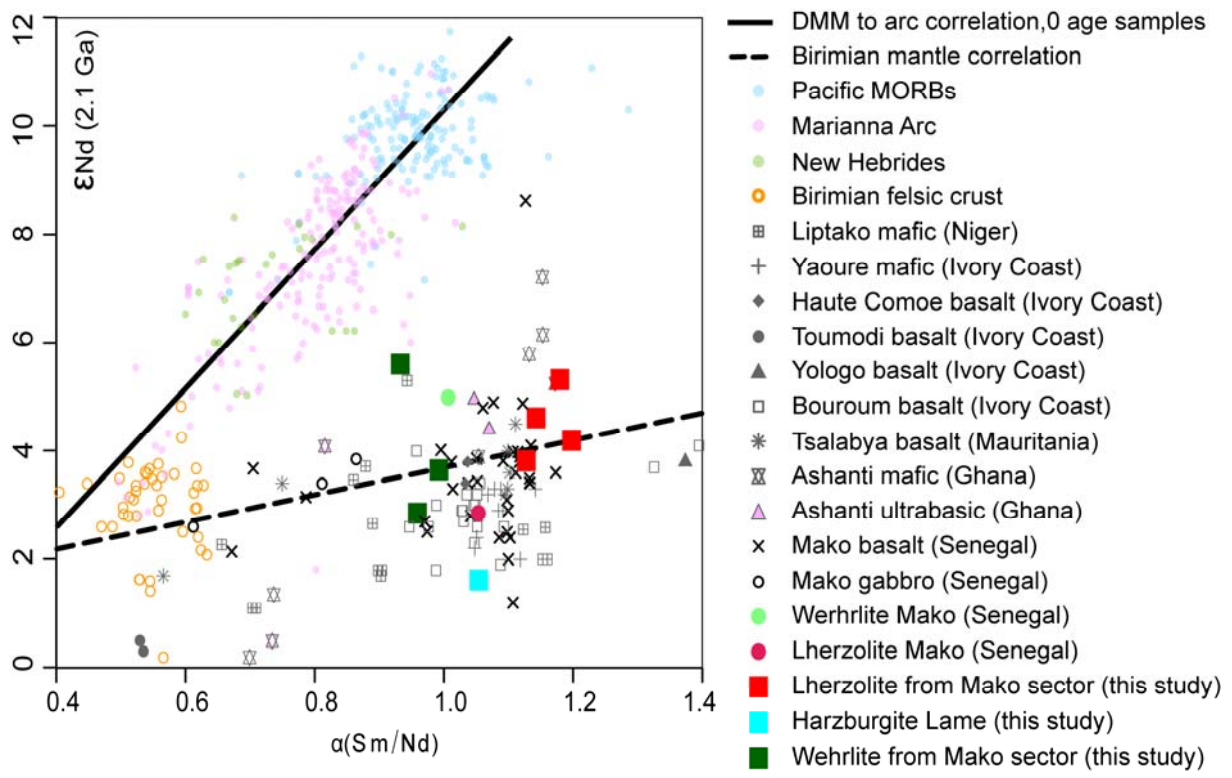


Table 7

Locality	Mako															
Mineralogy	Cpx															
Lithology	Lhz													Whr		
Sample	IL10	IL10	IL10	IL10	IL10	136	136	136	136	136	ILL4	ILL4	116	ILL3	ILL3	
Rb	<0.161	<0.26	0.237	<0.22	<0.23	<0.30	0.47	<0.44	<0.42	<0.44	<0.42	<0.41	0.56	<0.53	<0.37	
Ba	0.237	0.3	<0.139	1.19	0.7	0.89	0.41	<0.63	0.72	<0.55	0.84	0.94	0.6	<0.69	0.95	
Th	0.019	0.023	0.004	0.002	0.004	<0.00	<0.008	<0.00	<0.012	0.015	0.087	0.050	0.007	0.019	<0.007	
U	<0.002	0.010	0.002	0.002	<0.00	<0.00	<0.00	<0.005	<0.00	<0.00	0.021	0.009	<0.005	<0.00	0.008	
Nb	0.096	0.128	0.104	0.038	<0.029	<0.040	0.054	<0.049	0.065	0.063	0.109	<0.059	0.066	<0.065	<0.041	
La	0.61	0.83	0.286	0.36	0.276	0.25	0.156	0.145	<0.074	0.182	1.02	0.86	0.55	0.134	0.45	
Ce	2.48	3.01	1.10	1.19	1.01	1.00	0.68	0.61	0.53	0.74	3.12	2.68	1.48	0.64	1.89	
Pb	0.052	<0.040	0.053	0.049	0.108	<0.055	<0.049	0.103	0.075	<0.061	0.144	0.228	0.08	<0.079	0.136	
Pr	0.56	0.63	0.225	0.259	0.211	0.25	0.172	0.132	0.135	0.18	0.55	0.5	0.26	0.149	0.4	
Sr	14.91	9.64	13.98	11.17	10.25	10.34	8.49	8.48	8.22	11.56	13.68	12.95	7.37	7.75	12.79	
Nd	3.37	3.69	1.47	1.74	1.33	1.65	1.23	0.84	1.01	1.26	2.91	2.81	1.238	1.08	2.63	
Zr	11.46	14.25	4.19	6.87	3.96	2.84	3.85	3.56	1.19	1.89	10.1	9.34	4.09	3.9	9.38	
Sm	1.38	1.51	0.55	0.682	0.495	0.75	0.54	0.33	0.43	0.49	1.01	1.01	0.42	0.44	1.05	
Eu	0.436	0.396	0.228	0.279	0.204	0.3	0.245	0.147	0.183	0.197	0.41	0.41	0.167	0.2	0.47	
Ti	2148	2744	1530	2219	1604	1824	1798	1139	1208	1272	2792	2985	1265	1085	2517	
Dy	2.43	2.04	1.01	1.32	0.94	1.31	1.19	0.75	0.79	0.81	2.03	2.05	0.68	0.91	2.25	
Ho	0.53	0.43	0.219	0.3	0.202	0.25	0.26	0.138	0.145	0.139	0.47	0.48	0.14	0.21	0.51	
Er	1.33	1.05	0.62	0.9	0.59	0.68	0.71	0.34	0.35	0.33	1.44	1.46	0.404	0.6	1.55	
Y	13.79	14.74	7.52	10.81	7.31	7.06	7.94	4.34	4.39	4.82	17.02	16.9	6.26	5.59	12.95	
Yb	1.25	1.03	0.63	0.91	0.59	0.61	0.64	0.28	0.29	0.27	1.45	1.47	0.405	0.61	1.56	
Lu	0.165	0.138	0.092	0.135	0.09	0.086	0.083	0.038	0.039	<0.056	0.224	0.226	0.058	0.085	0.225	
Tb	0.405	0.342	0.149	0.188	0.134	0.199	0.168	0.108	0.122	0.129	0.286	0.284	0.101	0.14	0.33	
Ta	0.021	<0.026	<0.014	0.020	<0.021	<0.037	<0.043	<0.055	<0.053	<0.061	<0.046	<0.045	<0.053	<0.056	<0.054	
Hf	0.36	0.425	0.156	0.283	0.177	0.155	<0.158	<0.128	<0.149	0.162	0.149	0.155	0.118	0.18	0.57	
Σ REE	131.16	124.55	57.83	75.23	53.47	66.71	57.51	33.84	36.66	36.66	125.95	123.46	45.94	49.20	123.53	
(La/Yb)ch	0.46	0.76	0.43	0.37	0.44	0.39	0.23	0.49	0.64	0.66	0.55	1.28	0.21	0.27		
(La/Sm)ch	0.32	0.39	0.37	0.38	0.40	0.24	0.21	0.31	0.27	0.72	0.61	0.94	0.22	0.31		
(Tb/Yb)ch	1.66	1.71	1.21	1.06	1.17	1.68	1.35	1.98	2.16	2.45	1.01	0.99	1.28	1.18	1.09	
(La/Nd)ch	0.39	0.49	0.42	0.45	0.45	0.33	0.28	0.38	0.31	0.76	0.67	0.97	0.27	0.37		
(Sm/Tb)ch	0.87	1.13	0.95	0.93	0.95	0.97	0.82	0.78	0.90	0.97	0.91	0.91	1.07	0.81	0.82	
(Dy/Lu)ch	1.75	1.76	1.30	1.16	1.24	1.81	1.70	2.35	2.41	1.08	1.08	1.39	1.27	1.19		
Eu/Eu*	0.68	0.64	0.93	0.91	0.92	0.90	0.94	0.90	0.93	0.91	0.89	0.89	0.94	0.93	0.93	

